ABSTRACT

JOIJODE, ABHAY SHAM. Behavior and Properties of Self-Nucleated Poly (ethylene terephthalate) (PET). (Under the direction of Dr. Alan E. Tonelli).

The chemistry/microstructures of polymers determine their potential range of properties, but their collective organization in the bulk determines how much of this potential can be realized for various applications. Many polymers have limitations due to their random coiled and entangled structures, which result in lower degrees of crystallinity. Reorganization of the polymer chains to achieve largely extended and unentangled conformations can serve to overcome these limitations.

Bulk as-received poly (ethylene terephthalate) (asr-PET) has been observed to reorganize both morphologically and conformationally, either by formation of a crystalline inclusion compound (IC) between guest PET and host γ-cyclodextrin (γ-CD), followed by removal of the host γ-CD and coalescence of the guest PET (c-PET), or by precipitation (p-PET) from its solution in trifluoroacetic acid upon gradual addition into a large excess of rapidly stirred acetone. c-PET and p-PET show similar behavior, but p-PET can be more easily produced in larger quantities. Differential Scanning Calorimetry (DSC) observations of p-PET imply structures and morphologies different from those of asr-PET obtained by standard processing techniques. In comparison with the as-received PET, p-PET crystallizes rapidly from the melt, and, upon heating, its amorphous domains do not show any glass transition or crystallization peaks, but only a melting peak. These DSC observations suggest that p-PET attains higher crystallinity even when repeatedly cooled rapidly from the melt. The extended conformations of unentangled chains in p-PET do not become coiled and entangled even after spending substantial time in the melt.

As a consequence, we have demonstrated that p-PET can be used in small quantities as an effective self-nucleating agent to control the bulk semi-crystalline morphology of melt-processed PET, and the resulting properties of nucleated PET (nuc-PET) have been assessed. The nucleated polymer could be used for various applications in textiles and food packaging, with significant advantage over those obtained with normal asr-PET.

Behavior and Properties of Self-Nucleated Poly (ethylene terephthalate) (PET)

by
Abhay Sham Joijode

A thesis submitted to the Graduate Faculty of
North Carolina State University
in partial fulfillment of the
requirements for the degree of
Master of Science

Textile Chemistry

Raleigh, North Carolina

2011

APPROVED BY:

Dr. Alan E. Tonelli Committee Chair	Dr. Russell E. Gorga
Dr. Jan Genzer	

DEDICATION

I dedicate this work to my loving parents, sister and friends for their support and confidence in my capabilities.

BIOGRAPHY

Abhay Sham Joijode was born in Mumbai, India and he completed his Bachelors of Technology degree in Fiber and Textile Processing Technology at Institute of Chemical Technology (formerly UDCT) from Mumbai, India.

With research interests in fiber and polymer science he joined the research group of Dr. Alan E. Tonelli after getting admission to North Carolina State University for his Master's Degree in Textile Chemistry.

Since then he has been an active member of this group investigating structure property relations in polymers mainly processed with cyclodextrins.

ACKNOWLEDGMENTS

I would like to thank the chair of my advisory committee Dr. Alan E. Tonelli for his support during my master's program. I would also like to thank the members of the advisory committee; Dr. Russell E. Gorga and Dr. Jan Genzer.

I would like I would like to specially thank Dr. Richard J. Spontak for his help with the permeability tests, Mangesh Champhekar for helping me with nano-indentation tests and Birgit Anderson and Judy Elson for their help in training me with the analytical instrumentation. Additionally, I would also like to acknowledge the past and current members of my research group for their help and co-operation during my master's research work.

TABLE OF CONTENTS

List of Tables.....vii

List of Figures.....viii

Chapter 1: Background.....1

1.1 Poly (ethylene terephthalate) (PET) and its Properties.....1

1.2 Crystallization in PET.....3

1.3 Modifying PET to improve its Crystallinity.....6

1.3.1 Cold Drawing, Annealing and Heat Setting.....6

1.3.2 Solvent Induced Crystallinity.....8

1.3.3 PET coalesced from its γ-cyclodextrin Inclusion Complex.....9

1.4 Crystallization in PET via Nucleation.....15

1.5 Motivation.....18

Chapter 2: Methods and Materials.....20

2.1 Materials.....20

2.2 Experimental Methods.....20

2.2.1 PET Precipitation and Nucleation.....20

2.2.2 Fourier Transform Infrared Spectroscopy (FTIR).....21

2.2.3 Differential Scanning Calorimetry (DSC).....23

2.2.4 Film Preparation.....25

2.2.5 Density Measurements.....25

2.2.6 Nano-indentation.....26

2.2.7 Polarized Optical Microscopy (POM).....27

2.2.8 Gas Permeability Tests.....28

Chapter 3: Results and Discussions.....30

3.1 FTIR Analysis of As-received and Precipitated PET.....30

3.2 Thermal behavior of As-received and Precipitated PET.....31

3.3 Thermal Behavior of Self-Nucleated PET and Mechanism of Nucleation.....36

3.4 Evaluation of Self-Nucleation: p-PET vs. Traditional nucleating agents.....38

3.5 PET Densities.....42

3.6 Nano-indentation of PET Films.....44

3.7 Polarized Optical Microscopy (POM).....47

3.8 Gas Permeability Tests.....48

3.9 Repeated Self-Nucleation.....51

Chapter 4: Conclusions.....53

Chapter 5: Future Work and Potential Applications.....55

References.....57

LIST OF TABLES

Table 1: The trade names of PETs and their manufacturers.....2

Table 2: Physical and Chemical Properties of PET.....3

Table 3: Structural Properties of Cyclodextrins.....10

Table 4: Heating Runs I and II DSC data for different PET samples.....15

Table 5: Results for PET nucleated with various additives.....17

Table 6: DSC data for as-received and precipitated PETs.....33

Table 7: Densities of asr-PET and nuc-PET.....43

Table 8: CO2 (0.2MPa) solubility, diffusivity and permeability in PET films.....50

LIST OF FIGURES

Figure 1: Synthesis of PET via Polycondensation.....1

Figure 2: DSC scan of PET in heating cycle.....4

Figure 3: Effect of solvent treatment time on the induced crystallinity in PET.....8

Figure 4: Structures and molecular dimensions of Cyclodextrins.....9

Figure 5: Polymer Processing with Cyclodextrins.....11

Figure 6: Crystal Arrangement of Cyclodextrins.....12

Figure 7: PET coalesced from its γ-cyclodextrin Inclusion Complex.....13

Figure 8: DSC scans of as-received PET runs I (a) and II (b), solution-cast PET runs I (c) and II (d), and IC-coalesced PET runs I (e) and II (f).....14

Figure 9: Structural Reorganization from random coils to extended chains.....19

Figure 10: Schematic representation of the preparation of Precipitated PET.....20

Figure 11: Topographic view of sample after indentation.....27

Figure 12: Schematic of the Magnetic Suspension Balance.....29

Figure 13: FTIR spectra for asr-PET and p-PET.....30

Figure 14: DSC scans for as-received PET.....31

Figure 15: DSC scans for precipitated PET.....32

Figure 16: Conformational Changes in PET.....35

Figure 17: DSC scans for Self-Nucleated PET.....36

Figure 18: Mechanism of Self-Nucleation in 5:95 p-PET:asr-PET to form nuc-PET.....37

Figure 19: DSC thermograms of asr-PETs nucleated with a) 5% γ-cyclodextrin b) 30% glass particles and c) 5% talc.....39

Figure 20: Percentage crystallinity in asr-PET nucleated with different nucleants.....41

Figure 21: DSC Heating Scans for a) asr-PET and b) nuc-PET.....42

Figure 22: Loading-unloading nano-indentation curve for asr-PET sample.....44

Figure 23: a) Hardness and b) Young's Moduli for asr-PET and nuc-PET films.....46

Figure 24: Polarized Optical Micrographs of a) asr-PET and b) nuc-PET.....47

Figure 25: CO_2 absorption curves for asr-PET (above) and nuc-PET (below).....49

Figure 26: Repeated Self-Nucleation.....52

Figure 27: Structure-Property Relationships for nuc-PET.....54

CHAPTER 1: BACKGROUND

1.1 Poly (ethylene terephthalate) (PET) and its Properties

Polyesters were initially investigated during a fundamental research program at E. I. du pont de Nemours and Co (USA) by Carothers in 1929. Poly (ethylene terephthalate) (PET) was an aromatic polyester prepared by Whinfield and Dickson of the Calico Printers Association Ltd. (UK) and was later put to commercial scale manufacturing by E. I. du pont de Nemours and Co (USA) and Imperial Chemical Industries Ltd. (UK) in 1953 [1].

PET is synthesized by polycondensation reaction between ethylene glycol (EG) and dimethyl terephthalate (DMT) or terephthalic acid (TPA), though most of the commercial manufacturing processes make use of TPA. The polymerization is carried out around 280^{o} C in a continuous melt phase process. The polycondensation reaction is shown in Figure 1 [2].

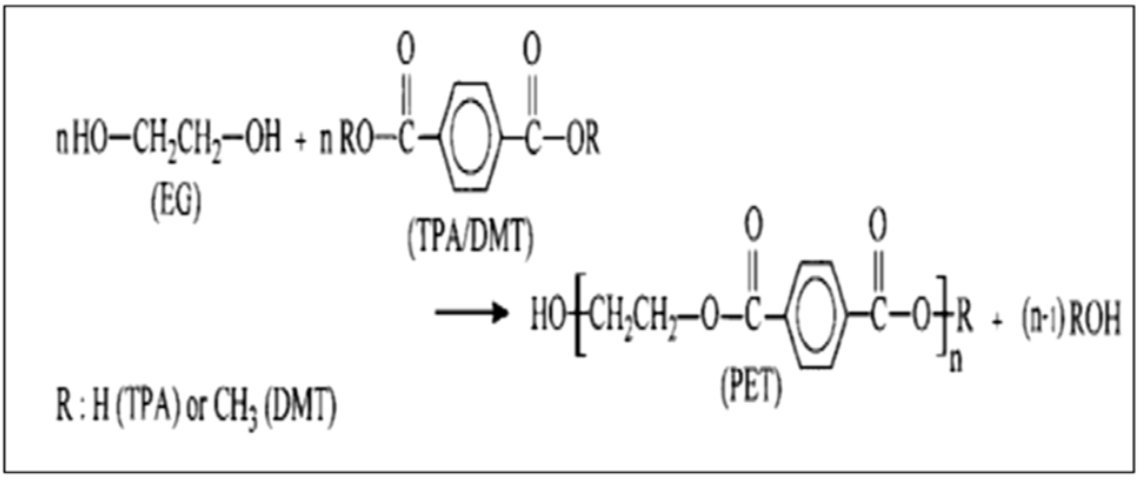

Figure 1: Synthesis of PET *via* Polycondensation

During synthesis, PET may undergo trans-esterification reactions at elevated temperatures, where interaction between two terminated polymer chains causes further chain

growth. This is critical from a material development point of view, as trans-esterification affects molecular weight and subsequently the resultant polymer properties.

PET is usually used in the form of fibers, films or sheets and finds major application in textiles and food packaging. Table 1 lists the manufacturers and trade names of commercial PETs [3].

Table 1: Trade names of commercial PETs and their manufacturers

Trade name	Manufacturer
Arnite	DSM Engineering Plastics
Diolen	ENKA-Glazstoff
Eastapac	Eastman chemical company
Hostadur	Farbwerke Hoechst AG
Mylar	E. I. Du Pont de Nemours & Co., Inc.
Melinex	Imperial Chemical Industries Ltd.
Rynite	Du Pont de Nemours & Co., Inc.

PET is an aromatic polyester and a semi-crystalline engineering thermoplastic polymer. It has good mechanical strength and can be melt- pressed in to clear films. It has low permeability to gases and good resistance to chemicals [4], and, so, PET is approved for food packaging applications. It has good frictional coefficient, dimensional stability, resistance to

wearing, electrical properties, optical clarity and excellent thermal properties [5]. Some of the properties of PET are mentioned in Table 2 [3].

Table 2: Physical and Chemical Properties of PET

Property	Test method	Value (unit)
Molecular weight (of repeating unit)	–	192 ($gmol^{-1}$)
Weight-average MW	–	30,000–80,000 ($gmol^{-1}$)
Density	–	1.41 (gcm^{3})
Glass transition temperature	DSC	69–115 (^{o}C)
Melting Temperature	DSC	245-265 (^{o}C)
Heat of fusion	DSC	120-166 (J/g)
Breaking strength	Tensile	50 (MPa)
Tensile strength (Young's modulus)	Tensile	1700 (MPa)
Yield strain	Tensile	4 (%)
Impact strength	ASTMD 256-86	90 (Jm^{-1})
Water absorption (after24h)	–	0.5 (%)

Thus, PET is characterized by good all round properties which makes it commercially important.

1.2 Crystallization in PET

The semi-crystalline morphology of PET influences its behavior and properties. More specifically, its inability to readily crystallize makes it distinct from most other polymers. PET can be characterized by various analytical techniques such as Differential Scanning

Calorimetry (DSC), X-ray Diffraction, Fourier Transform Infrared Spectroscopy (FTIR), Nuclear Magnetic Resonance (NMR), etc., but DSC is most commonly employed to study the thermal and crystallization behaviors of semi-crystalline polymers like PET.

DSC helps us understand the thermal transitions in polymers, like glass transition, and crystallization and melting behaviors. Crystallization in polymers determines the resultant morphologies and properties. Hence it is important to understand the crystallization mechanism of PET, as it plays an important role in product development [6]. A typical DSC thermogram of PET recorded during heating is shown in Figure 2 [7].

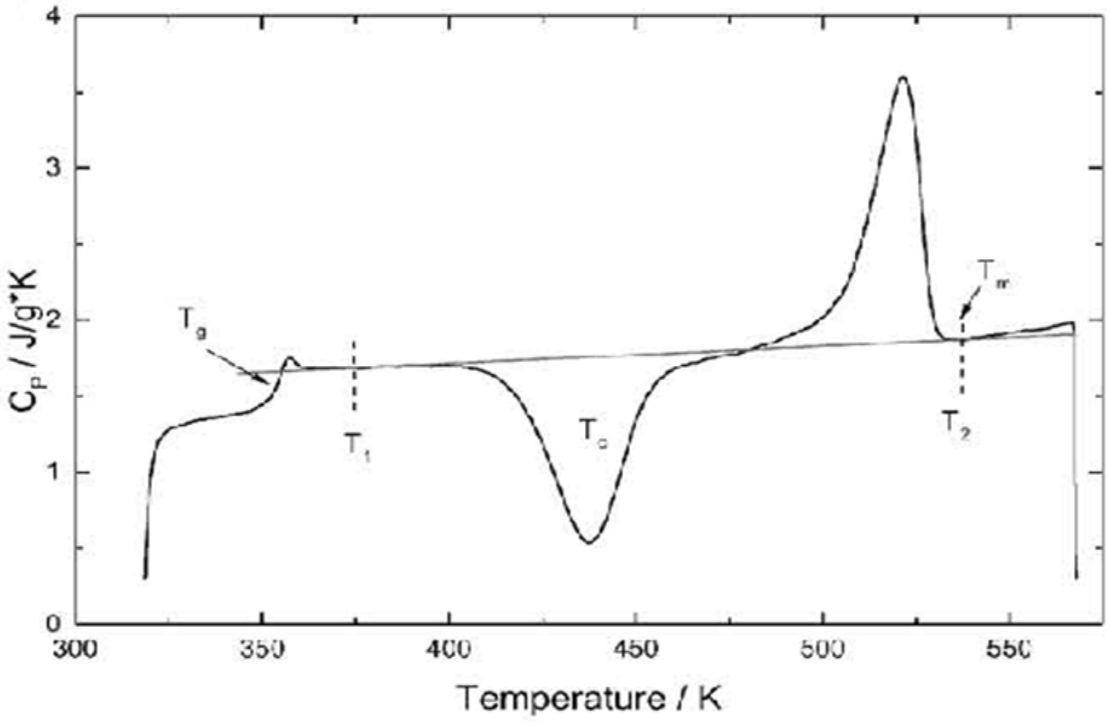

Figure 2: DSC of PET in heating cycle

This is a DSC thermogram typical of many semi-crystalline polymers, exhibiting a glass transition, T_g, wherein the polymer chains transition from a glassy to a rubbery phase induced

by chain mobility. This is followed by a secondary crystallization exotherm, and finally the polymer melts at T_m into an amorphous liquid. PET cooled rapidly from the melt to below T_g develops little crystallinity, which is subsequently produced during slower heating above T_g. When PET is heated above its T_g , the polymer chains absorb the heat energy and become mobile. They can then move closer to each other in a folded pattern to crystallize. Crystallization upon heating limits the temperature range at which this amorphous PET can be used since there is change in its material properties upon heating.

Crystallinity in PET can be evaluated using the heats of crystallization and melting observed in a DSC heating scan. The amount of crystallinity in the polymer is the ratio of the difference in heat of melting and heat of crystallization to the theoretical heat of melting for 100% crystalline PET. A range of values for ΔH_m^* are recorded in literature but we will be using ΔH_m^*=140 J/g (at 280^o C) for our analysis [8].

$$\textbf{Crystallinity } (X_c) = (\Delta H_m - \Delta H_c)/\Delta H_m^*$$

ΔH_m – Heat of Melting (J/g)

ΔH_c – Heat of Crystallization (J/g)

ΔH_m^* – Theoretical Heat of Melting (J/g)

Another method used to determine crystallinity in PET is with density measurements. In this technique the density of the sample can first be evaluated using a floatation method. The PET sample is subjected to a mixture of non-solvents (NSs). One of the non-solvents has a density lower and other non-solvent higher than that of PET. The experimental density is calculated as follows,

$$\rho_{exp} = \frac{[\text{volume(NS 1)x}\rho\text{(NS 1)} + \text{volume(NS 2)x}\rho\text{(NS 2)}]}{\text{volume(NS 1)} + \text{volume(NS 2)}},$$

The crystalline and amorphous densities for PET are ρ_c = 1.515 g/cm^3 and ρ_a = 1.335 g/cm^3 respectively [9, 10]. The fraction of crystallinity then can be calculated using the following equation [6],

$$X_c = (\rho_{exp} - \rho_a)\, \rho_c / (\rho_c - \rho_a)\, \rho_{exp}$$

ρ_{exp} – Measured density of the sample (g/cc)

ρ_a – Amorphous density of PET (g/cc)

ρ_c – Crystalline density of PET (g/cc)

Primary crystallization in PET is dependent on the cooling rate from the polymer melt. In most of the commercial processes involving PET, the polymer is rapidly quenched into ice water. This involves cooling the polymer from its melt at extremely high cooling rates. The polymer chains do not adjust to this sudden change and therefore are not able to reorganize and crystallize. Hence, as a result primary crystallization is largely absent and the rapidly quenched material is mostly amorphous. Due to the slow crystallizing nature of PET it inadvertently has low crystallinity, and to improve its properties for various applications PET needs to be modified both morphologically and conformationally.

1.3 Modifying PET to Improve its Crystallinity

1.3.1 Cold Drawing, Annealing and Heat Setting

Cold drawing is a process usually applied to PET fibers, wherein the crystallinity is partially improved by drawing the fibers through a set of rollers. In this technique the fibers

after being spun through a spinneret are taken up over a series of rollers where the rotational speed of the lead roller is higher than the preceding roller. This applies a stretch to the fibers causing molecular alignment due to viscous flow thereby increasing crystallinity. Cold drawing is usually done below the glass transition temperature and the strain rates applied are well below the breaking strain limit. The issue with cold drawn PET is that it tends to undergo large shrinkage upon heating as the stretched polymer chains absorb energy and return to their preferred non-oriented coiled state [11].

Annealing is a process in which the polymer is heated above its glass transition temperature. The polymer chains are mobile to some extent due to the absorbed heat and tend to crystallize. It has been found that the *Trans* to *Gauche* conformation ratio increases as the annealing temperature rises, because during crystallization the ethylene glycol -CH_2–CH_2- bonds transform from predominantly *Gauche* to *Trans* [12]. The heat setting technique is similar to annealing and was developed to address PET shrinking on heating. This technique is applied to fibers and films and involves heating PET above its glass transition temperature. In heat setting the polymer is held in its stretched condition at its crystallization temperature for a certain period of time. The polymer chains are oriented and are not allowed to shrink at this elevated temperature, thereby improving its crystallinity. This creates some sort of memory for the polymer chains to remain oriented even when heated to beyond its crystallization temperature to near its melting temperature [13]. Cold drawing, annealing, and heat setting are all physical processes in which the crystallinity is improved by orientation, but the crystallinity that is induced is rapidly lost upon melting.

1.3.2 Solvent Induced Crystallinity

Crystallinity in PET can also be improved by treating it with solvents like acetone that induce crystallinity due to their absorption in the amorphous domains. This increases the crystallinity as a result of reduction in glass transition temperature, which facilitates chain mobility [14]. Crystallization during solvent treatment occurs due to structural reorganization leading to alignment of crystallites. Also the rate of crystallization linearly increases with the solvent temperature [15].

Solvent induced crystallinity was found to be dependent on the solubility parameter. It has been shown that solvents which have solubility parameters similar to the polymer are more efficient in increasing crystallinity [16]. Also the amount of solvent used [17, 18] and solvent treatment time are directly proportional to the induced crystallinity. Figure 3 illustrates the effect of solvent treatment time on the induced crystallinity in PET [16].

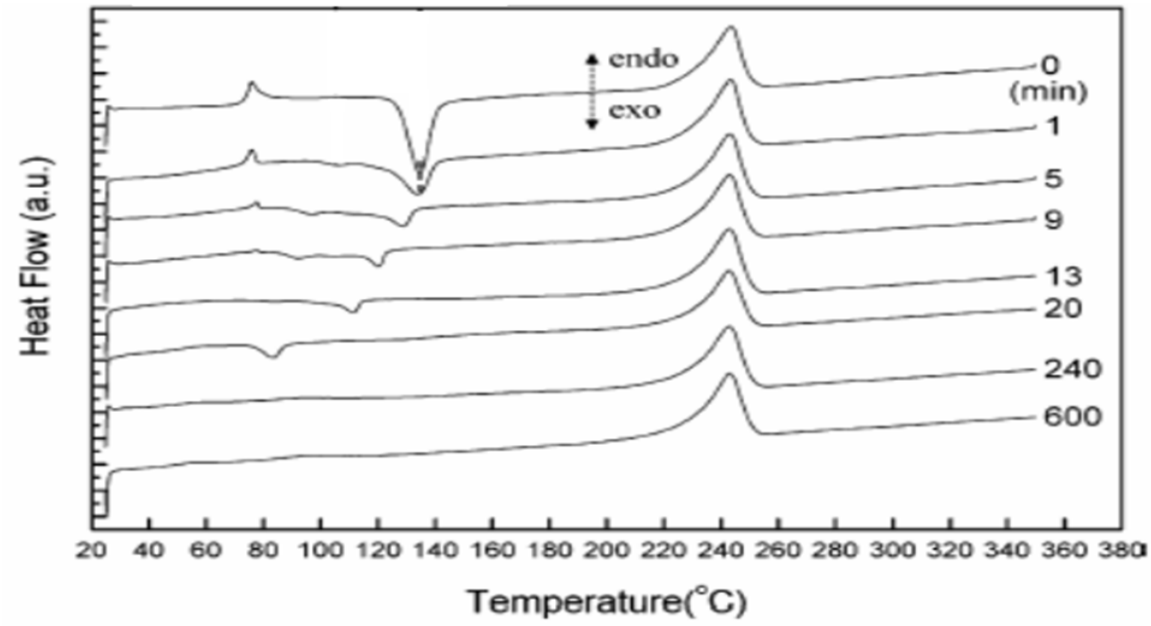

Figure 3: Effect of solvent treatment time on the induced crystallinity in PET

1.3.3 PET coalesced from its γ-cyclodextrin Inclusion Complex

Cyclodextrins are cyclic starches and were first discovered by A. Villiers [19]. Schardinger later on separated α and β cyclodextrins [20], while γ-cyclodextrin was discovered by Freudenberg and Jacobi [21]. α, β and γ cyclodextrins are the three commercially known cyclic starches with six, seven and eight glucopyranose units respectively [22]. Figure 4 shows the structures and molecular dimensions of cyclodextrins (CDs) and Table 3 lists their structural properties.

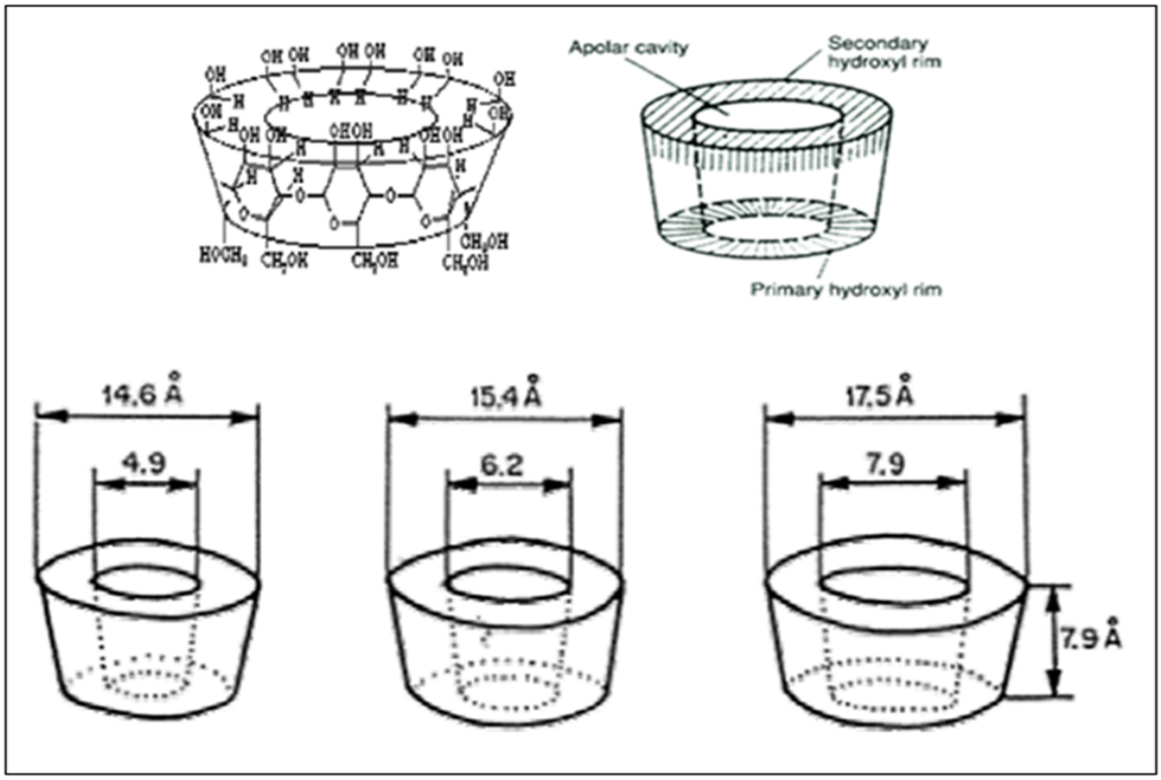

Figure 4: Structures and molecular dimensions of CDs

The inner cavities of CDs contain carbon and oxygen from the ether linkages, rendering it relatively hydrophobic, while the outer edges contain the hydroxyl groups making them hydrophilic in nature [23].

When an aqueous solution of cyclodextrin comes in contact with a polymer solution the water in the hydrophobic cavity often gets replaced by the polymer chains thereby forming an inclusion complex. During the inclusion process there is simultaneous diffusion of

Table 3: Structural Properties of Cyclodextrins [23]

Cyclodextrin	**α**	**β**	**Γ**
Number of glucose units	6	7	8
Molecular Weight	972	1135	1297
Inner Diameter (nm)	0.45-0.57	0.62-0.78	0.79-0.95
Outer Diameter (nm)	1.37	1.53	1.69
Height (nm)	0.79	0.79	0.79
Cavity Volume (nm^3)	0.174	0.262	0.472
Crystal Forms	Hexagonal plates	Monoclinic parallelograms	Quadratic Prisms

polymer chains and cyclodextrin followed by threading of the chains, which generally leads to precipitation of a crystalline polymer-cyclodextrin inclusion complex (polymer-CD-IC). Thus there is nano-threading of the guest polymers chains through the host CDs.

When the polymer-CD-IC is washed to remove the host CDs the resultant coalesced guest polymer has properties distinct from those of the as-received polymer. This results from changes in the bulk coalesced sample from entangled random coils to un-entangled extended chain morphologies and conformations. Figure 5 illustrates polymer nano-threading and restructuring *via* the cyclodextrin inclusion and coalescence techniques, respectively.

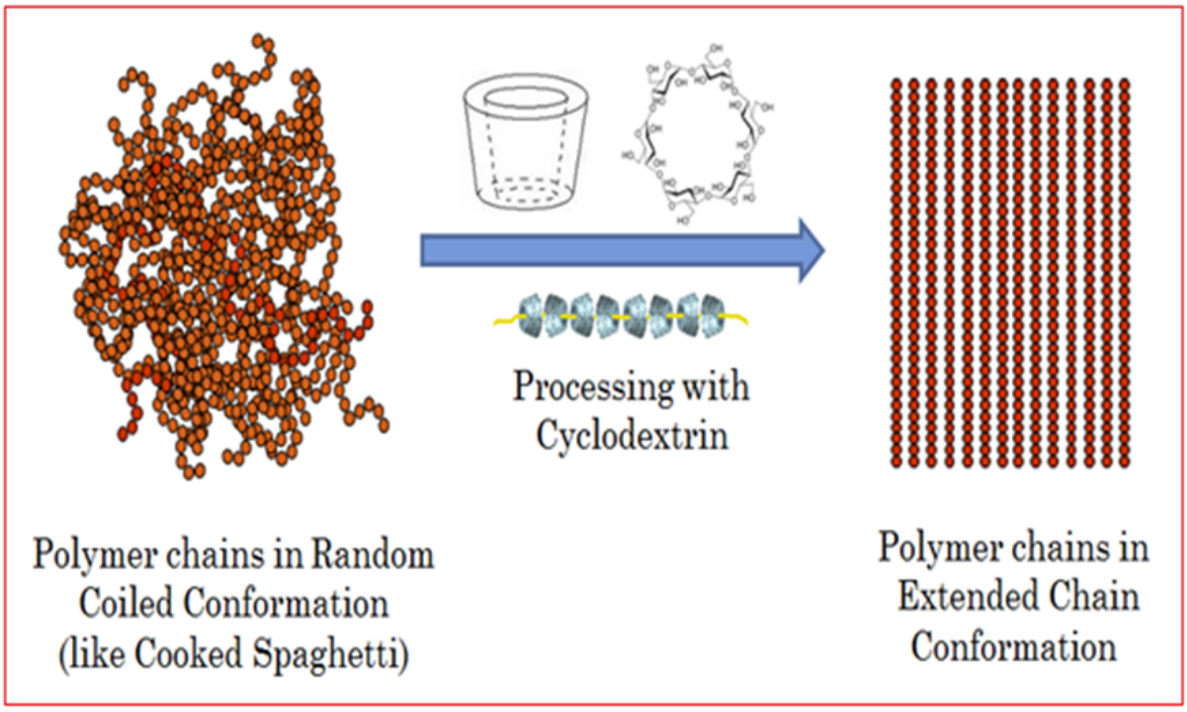

Figure 5: Polymer Processing with Cyclodextrins

Cyclodextrins crystallized from their aqueous solutions organize themselves into a cage like structure, and their arrangement is not a channel structure with cyclodextrins packed in head to tail columnar stacks as in polymer-inclusion complexes. Though not shown, this is

evident from their respective distinct X-ray diffraction patterns [24]. These crystal structures are shown in Figure 6.

Thus, polymers can be restructured using cyclodextrins to alter their morphology from entangled random coils to un-entangled extended chains and this change in conformation and morphology improves properties, specifically the crystallinity of the resultant polymer. Unlike the previously mentioned techniques of polymer processing, this enhanced crystallizability is not lost upon repeated melt-processing.

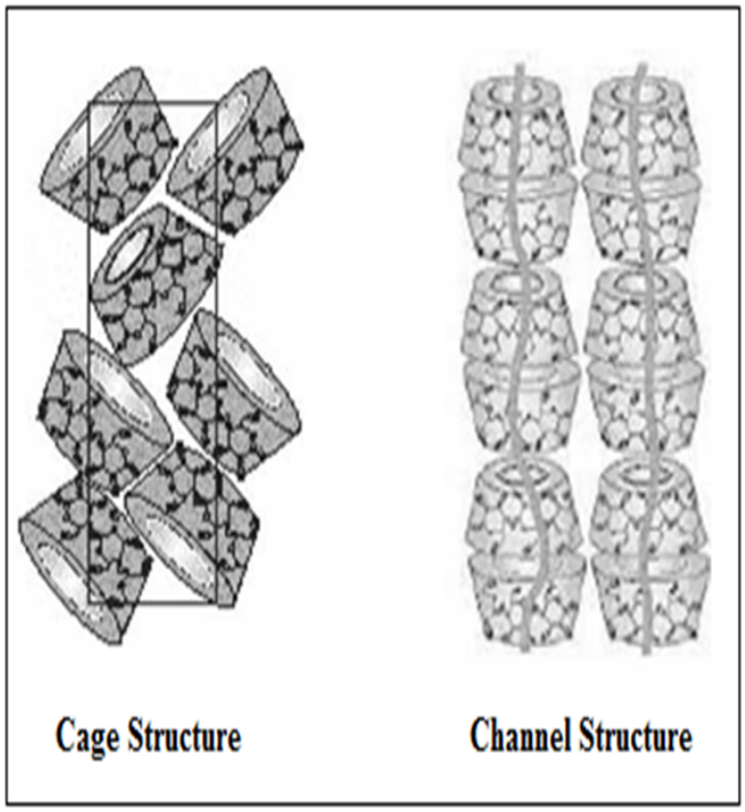

Figure 6: Crystal Arrangement of Cyclodextrins

PET can be restructured by coalescing it from its γ-cyclodextrin inclusion complex. This can be accomplished by dissolving PET in a solvent mixture at high temperature followed by

addition of saturated aqueous γ-cyclodextrin solution to the polymer solution. The resultant precipitate, which is the PET-γ-CD-IC, can be coalesced (c-PET) subsequently by washing it with hot water to remove the host γ-CD [25]. The inclusion complex formation and coalescence is illustrated in Figure 7 [26].

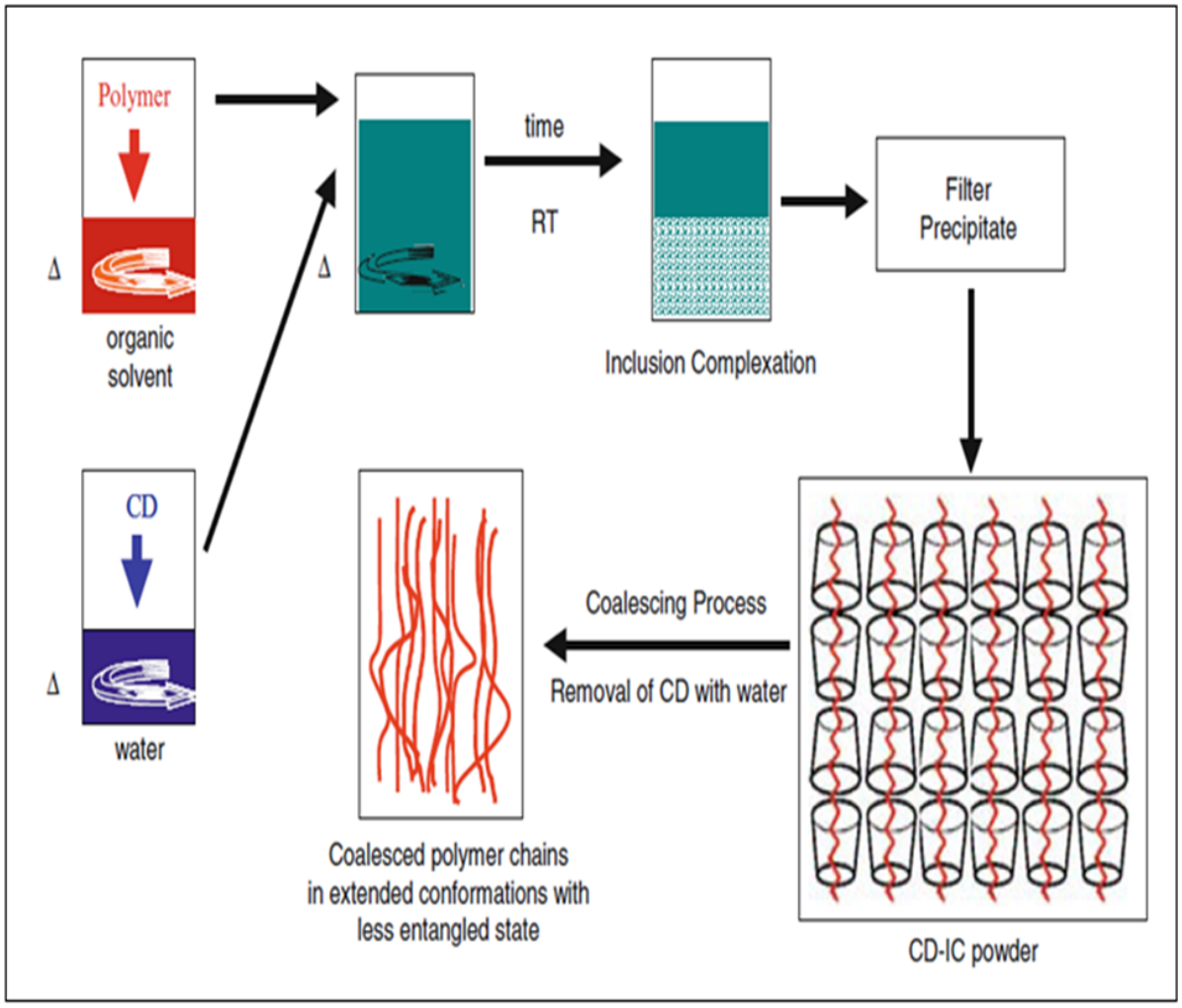

Figure 7: PET coalesced from its γ-cyclodextrin Inclusion Complex

PET is found to be reorganized differently when processed with cyclodextrin. c-PET has a higher crystallinity on account of its largely extended chain morphology. Owing to this fact, it does not evidence a glass transition or crystallization during DSC heating, but only a

melting peak. Repeated melting and rapid quenching does not seem to change this behavior which suggests that structural organization in c-PET is different from the as-received PET (asr-PET). Figure 8 compares the thermal behavior of c-PET with asr-PET and solution cast PET and Table 4 summarizes the DSC results [25].

FTIR and solid state ^{13}C NMR results for c-PET suggest that there is a conformational change due to the nano-threading process. WAXD data indicates that the diffraction pattern for c-PET is distinct from as-PET and is more similar to oriented PET. This tells us that c-PET has better orientation resulting in higher crystallinity [25].

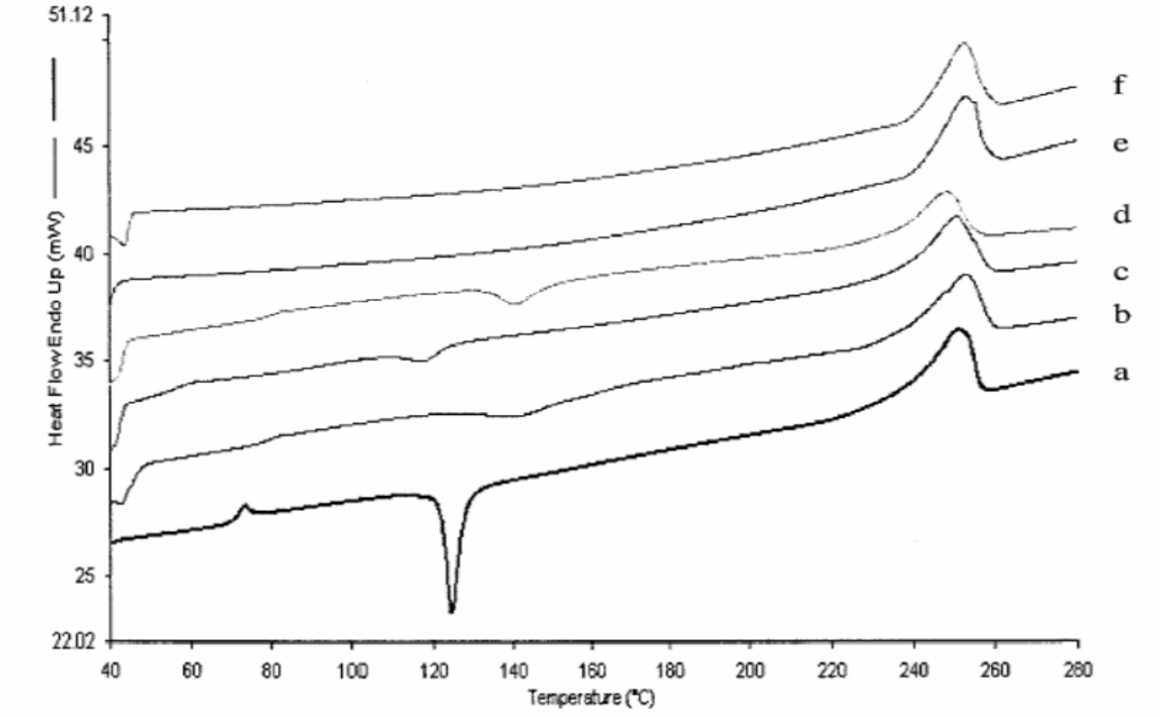

Figure 8: DSC scans of as-received PET runs I (a) and II (b), solution-cast PET runs I (c) and II (d), and IC-coalesced PET runs I (e) and II (f)

Todd Bullions et.al found that PET precipitated from its solution in a solvent mixture into a non-solvent has thermal and spectroscopic properties similar to those of c-PET [27]. The

behavior and properties of p-PET indicate that it has been structurally modified from asr-PET [28]. p-PET can also be repeatedly and rapidly crystallized from its melt without any change in its thermal behavior. This indicates that the precipitation method reorganizes PET into an extended chain conformation similar to the cyclodextrin inclusion/coalescence technique resulting in c-PET.

Table 4: DSC Heating Runs I and II data for different PET samples

	Crystallization				Melting			Difference	
Sample	T_g (°C)	Onset (°C)	T_c (°C)	ΔH_c (J/g)	Onset (°C)	T_m (°C)	ΔH_f (J/g)	$\Delta H_f - \Delta H_c$ (J/g)	W_c (%)
Pure PET run I	70.3	122.0	124.8	27.0	239.9	250.8	44.2	17.2	14.3
Pure PET run II	77.2	125.5	141.2	17.2	241.3	252.8	41.6	24.4	20.3
Cast PET run I	53.8	109.7	117.7	5.24	237.2	250.7	43.5	38.3	31.9
Cast PET run II	78.2	133.08	140.5	9.60	234.4	248.2	37.8	28.2	23.5
Coalesced PET run I	—	—	—	—	237.3	249.7	46.6	46.6	38.9
Coalesced PET run II	—	—	—	—	241.9	252.9	45.0	45.0	37.5

1.4 Crystallization in PET *via* Nucleation

PET is a slow crystallizing polymer and hence is hardly used in processes like injection molding. Due to its slow crystallizing nature, much effort has been made to enhance the crystallization rate in PET in order to achieve the desired morphology and properties. Addition of nucleating agents is the most common method to accelerate the crystallization rate, thereby enhancing both the applications and processing properties of PET [29]. Nucleating agents are generally crystalline additives that are usually insoluble in the polymer

melt and shorten the induction time and enhance the rate of crystallization from a molten phase [30]. They influence the spherulite size and distribution thus controlling the physical properties of the polymer. Nucleating agents can be divided in to three main categories; inorganic, organic and polymeric additives. The effect of nucleation is dependent on the properties of the nucleating agents, such as particle size and geometry, surface structure and interfacial interaction with the polymer [29]. Bulk polymers which are melt-crystallized have non-uniform spherulite distributions, resulting in formation of some large crystallites that impart poor transparency and reduced impact strength. Polymers processed with nucleating agents have more uniform spherulite growth, which results in improved semi-crystalline morphologies and mechanical properties [31].

Nucleation can be either homogeneous or heterogeneous. In heterogeneous nucleation, incompletely melted crystals or foreign particles, which are an integral part of the polymer system, like catalyst, etc., can act as nucleation sites [32, 33]. As the polymer is cooled from its melt, crystal growth starts from these sites causing faster crystallization. Homogeneous nucleation is rare and is of less commercial significance. Heterogeneous nucleation, wherein the nucleation additive is insoluble in the polymer melt, is more widely observed. The nucleating agent lowers the free energy barrier for stable nucleus formation, which results in reduced surface free energy [33]. As the polymer melt is cooled, crystallization is preferentially and simultaneously initiated at sites where the nucleating particles are present, and is known as primary crystallization. Once crystallization is induced, the spherulite growth is propagated resulting in improved crystallinity in the polymer, due to the more uniform distribution in spherulite sizes [32].

PET can be nucleated with various common nucleating agents like talc, mica, titanium dioxide, silicon dioxide, calcium carbide, calcium oxide, lead fluoride, lead acetate, sodium benzoate, and sodium stearate. Metal salts and ionomers also act as effective nucleants for PET. Table 5 illustrates results for PET nucleated with various nucleating agents. Among the drawbacks of these nucleating agents are that they can be harmful to the body and the

Table 5: Results for PET nucleated with various additives [33]

Additive	Additive[a] (wt %)	$\bar{M}_w$ (GPC)	$\bar{M}_n$	$\bar{M}_n$ (IV)	$T_p k_2$[b] (°C)
None	0	79,000	33,000	24,500[c]	202–205
	0	22,000	10,000	8000[d]	202–206
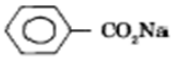	0.70	57,000	23,000	17,000	226.2
	0.94	36,000	15,000	14,500	230.3
	2.57	28,000	12,000	5300	237.6
$CH_3-(CH_2)_{16}CO_2Na$	2.10	32,000	13,000	12,800	230.3
Na_2CO_3	3.70	33,000	13,000	14,300	229.0
HCO_2Na	3.25	51,000	22,000	17,100	231.0
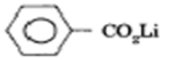	4.94	8300	3100	3000	226.0
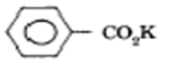	3.53	22,000	10,000	8000	229
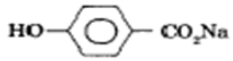	2.09	33,000	15,000	15,800	224.8
CH_3CO_2Na	15.65	32,000	14,000	17,000	224.0
	>10	56,000	18,000	17,000	225.3
Na_2SO_4	18.6	45,000	17,000	13,800	221.1
NaCl	14.60	61,000	24,000	21,900	216.5
	1.00	73,500	29,000	22,000	208.3
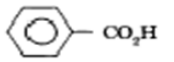	ca. 0.72	74,500	29,500	22,800	201.3–205.3

[a] Concentration of salt additive determined from atomic absorption measurements.
[b] $T_p k_2$: temperature at the peak of the exotherm on cooling from the melt.
[c] High molecular weight.
[d] Low molecular weight.

environment. Traditional heterogeneous nucleating agents cannot only be toxic, but they are also chemically incompatible with polymers, and as such complicate their recycling.

In this regard, the concept of bio-nucleation and self-nucleation become more critical and relevant for polymer nucleation. Bio-nucleation involves nucleating the polymers with environmentally friendly/responsible nucleating agents. These involve biodegradable nucleants like cyclodextrins. It was found that the non-stoichiometric (n-s)-polymer-CD-ICs provide environmentally safe, non-toxic nucleating agents for enhancing the melt crystallization of polymers to improve their physical properties. Non-stoichiometric inclusion complexes, i.e., (n-s)-polymer-CD-ICs, are obtained by excess addition of the guest polymer during the cyclodextrin inclusion process. The un-included dangling chains crystallize first during the cooling of the melt thus providing active sites for crystallization. Bio-nucleation of Nylon 6 was demonstrated by Mohan et al. with the use of non-stoichiometric nylon 6-α-CD inclusion complexes [34, 35]. Such bio-nucleating options will reduce hazardous buildup of toxins in the environment due to the reduced usage of traditional nucleating agents.

Self-nucleation results from the addition of modified PETs like c-PET or p-PET, whose behavior in the melt is different from asr-PET. Thus these restructured PET's can act as effective nucleating agents with advantages, such as complete chemical compatibility, non-toxicity and undetectable or "stealth" natures. In addition, they introduce no foreign material that would complicate PET recycling.

1.5 Motivation

PET is an aromatic semi-crystalline thermoplastic polymer and a versatile engineering plastic material with good all-round properties. It is commercially viable for numerous applications ranging from packaging and apparel to engineering components. PET is a slow crystallizing polymer and can be melt-quenched into a largely amorphous material. The

motivation of our research is to improve the properties of PET by structural modification, resulting in an un-entangled extended chain morphology, which is retained even when exposed to long times in the melt.

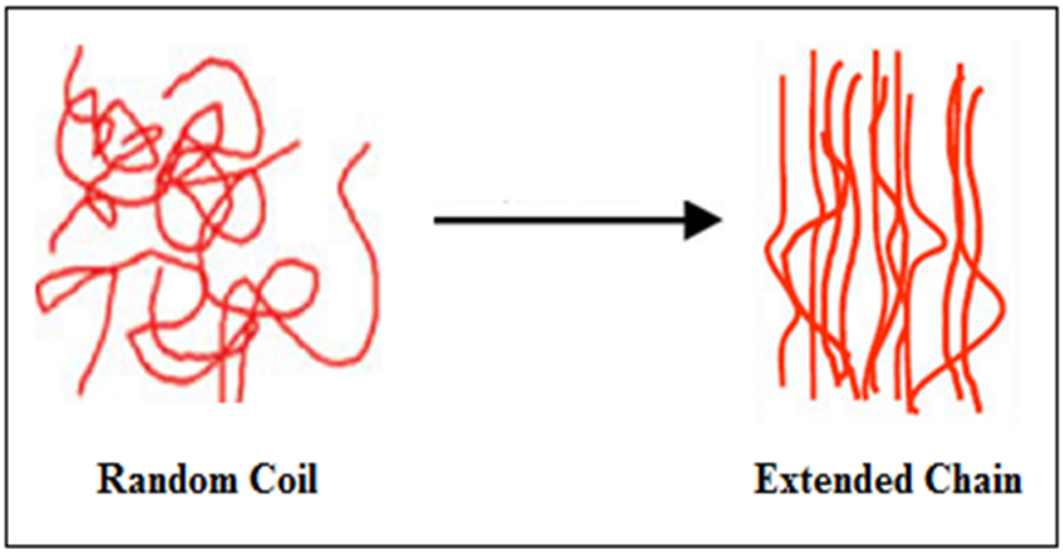

Figure 9: Structural Reorganization from random coils to extended chains

PET can be restructured from its entangled random coil morphology to largely un-entangled extended chain morphology, as illustrated in Figure 9, by coalescing it from its γ-cyclodextrin inclusion complex or by a precipitation technique. c-PET (coalesced from its γ–CD-IC) and p-PET (rapidly precipitated) exhibit such behavior, but it is easier to make p-PET in larger quantities. Hence, in this research structural reorganization of PET has been studied *via* the precipitation technique. P-PET has been demonstrated to be a self-nucleating agent for the melt-crystallization of asr-PET, and some resultant properties of such self-nucleated PET have been evaluated.

CHAPTER 2: MATERIALS AND METHODS

2.1 Materials

Poly (ethylene terephthalate) (M_v ~ 18,000, Virgin PET) and 30% Glass Reinforced PET), Trifluoro Acetic acid (TFA), Acetone, and Talc were obtained from Sigma-Aldrich while gamma cyclodextrin (γ-CD) was obtained from Cerestar (Hammond, IN).

2.2 Experimental Methods

2.2.1 PET Precipitation and Nucleation

PET was structurally modified by a precipitation technique [28]. Figure 10 broadly outlines the experimental procedure. About 3g of asr-PET were dissolved in 50 ml of Trifluoro Acetic acid (TFA), and the polymer solution was heated to 50°C with rapid stirring

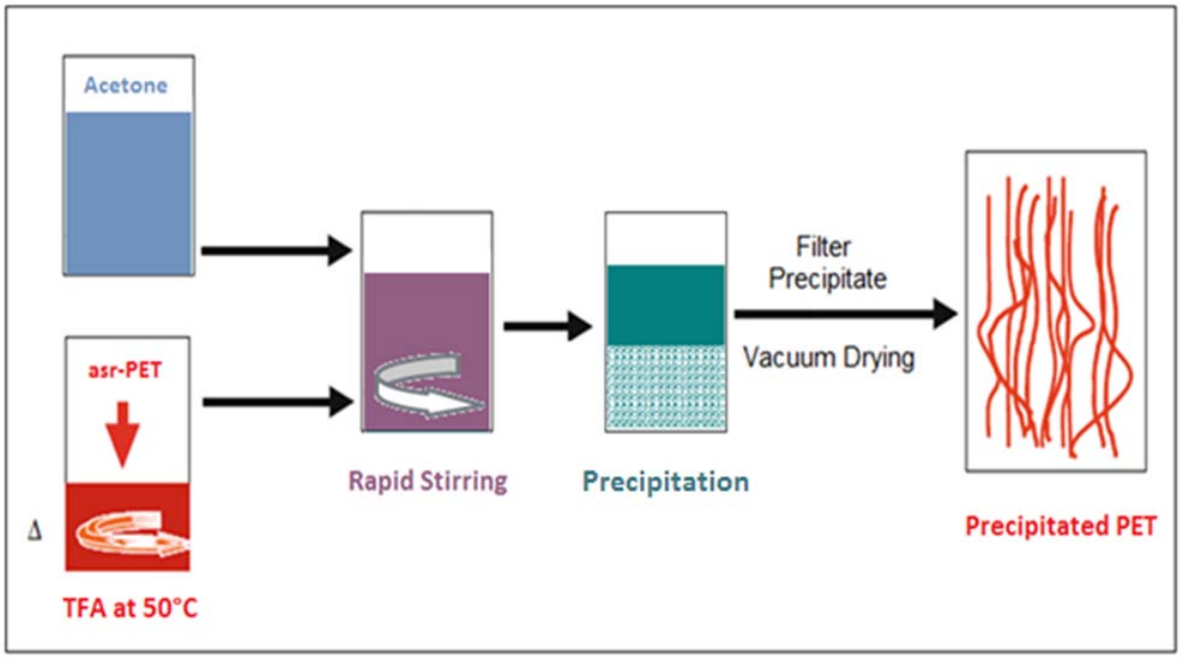

Figure 10: Schematic representation of the preparation of Precipitated PET

till the polymer completely dissolved (approximately 30 minutes). Then the heated polymer solution was gradually added drop wise to 150 ml of acetone while the mixture was stirred at a high rate. A white precipitate of the polymer (p-PET) is obtained at the end of the addition of the PET/TFA solution. The precipitate was then washed with acetone, filtered using Wattman filter paper under vacuum and dried in a vacuum oven overnight at 40° C to obtain dry precipitated PET. Flow times measured for 0.2 g/dL TFA solutions of asr- and p-PETs in a Fenske viscometer were closely similar, suggesting that the precipitation process did not cause any serious PET degradation. Finally, both asr-PET and p-PET were characterized for their resultant behaviors.

The asr-PET was nucleated using p-PET by a solvent casting method. In this technique asr-PET was initially dissolved in TFA. Then 5% (weight basis with respect to asr-PET) of p-PET was added to the solution when about two thirds of the solvent was evaporated. It was observed that p-PET did not dissolve in this concentrated polymer solution. A film of nucleated PET (nuc-PET) was obtained after complete solvent evaporation. To observe and evaluate the nucleating ability of p-PET with respect to traditional nucleating agents, asr-PET was nucleated with 5% γ-cyclodextrin (bio-nucleating agent), 5% talc (traditional nucleating agent) and PET with 30% glass reinforcement (commercially available nucleated PET). The percentage crystallinity in each case was calculated from their respective DSC thermograms, and the nucleation ability of each nucleating agent was evaluated by comparing the percentage crystallinity in the nucleated polymers.

2.2.2 Fourier Transform Infrared (FTIR) Spectroscopy

Fourier Transform Infrared (FTIR) Spectroscopy is a non-destructive polymer characterization technique that provides information about their chemical bonding and molecular structure. This analytical technique works on the principle of the vibrations of chemical bonds occurring at their characteristic frequencies. When the polymer specimen is subjected to a modulated IR beam it absorbs infrared energy at frequencies that are characteristic to that molecule and the sample's vibrational pattern at different frequencies is transformed into an IR absorption plot as a function of wave number. The resulting FTIR spectrum is then analyzed and usually compared with the FTIR library to get a spectral match in order to identify the polymer.

The instrument consists of an IR and laser source, interferometer, sample compartment and detector. A series of mirror assemblies direct the beam to different parts in the instrument as per requirement. The instrument has a frequency range of $500cm^{-1}$ to $4000cm^{-1}$ and the resolution can be varied from 0.5 cm^{-1} to 32 cm^{-1}. The sample compartment is purged to remove the effect of the presence of moisture and CO_2 on the spectrum.

The source in this instrument is infrared energy (Globar), and passes through an aperture which controls the energy presented to the sample. An Interferometer is an important part of the instrumental assembly. Radiation from the IR source is directed through the sample cell to a beam splitter. Half of the radiation is reflected from a fixed mirror while the other half is reflected from a mirror which moves continuously over a distance of about 2.5 micrometers. When the two beams are recombined at the detector, an interference pattern is produced. The Helium–Neon Laser introduced in the beam leaving the interferometer has a few important functions. Since IR is not detected by human eye, it permits us to place the sample in the

sample compartment exactly between the incident beam and the detector. It improves the accuracy of each measured frequency, and helps in synchronization of multiple scans. The beam from the sample goes to the DTGS detector which measures the interferogram signal and the measured signal is digitized and sent to the computer where the Fourier transformation takes place. The final infrared spectrum is then presented to the user for interpretation [35].

Absorption in the infrared region results in changes in vibrational and rotational status of the molecules. A molecule will absorb infrared light only if the absorption causes a change in the dipole moment. This results in a vibrational transition in the form of bending or stretching which occurs at a characteristic frequency that is specific for a particular bond or functional group.

Infrared spectral studies were conducted with a Nicolet Nexus 470 FTIR spectrometer in the range 4000 - 400 cm^{-1}, with a resolution of 4 cm^{-1} and 64 scans were collected for each sample. FTIR data were analyzed by using Omnic software.

2.2.3 Differential Scanning Calorimetry (DSC)

Differential Scanning Calorimetry (DSC) is based on the principle that the response of polymers varies with changes in temperature. DSC is a quantitative analytical tool that profiles caloric heat change from a sample pan with respect to a reference empty pan. A DSC thermogram helps in the analysis of thermal properties related to phase changes like glass transition, crystallization and melting behavior. It measures endothermic and exothermic heat flow in the polymer samples, which is done by monitoring the power (mW) required to maintain the sample and its pan at the same temperature as the reference pan. Prerequisite for

this instrument is the knowledge of thermal stability of the polymer sample, which can be obtained from Thermo-gravimetric analysis (TGA). TGA tells us about the percentage loss in weight of a polymer as a function of temperature. From TGA data a suitable temperature range should be chosen for DSC analysis in order to prevent sample degradation.

If a polymer sample absorbs energy when heated and becomes plastic due to chain mobility it shows an increase in its heat capacity. When the amorphous regions in the polymer become crystalline, they exhibit some energy release, which is an exothermic heat of crystallization. When the polymer reaches its melting temperature, it absorbs energy, resulting in an endothermic melting peak, and its molten chains become mobile and disordered resulting in an amorphous melt. All these transitions are recorded on a thermogram obtained from a differential scanning calorimeter.

DSC thermograms for PET were obtained using a Perkin-Elmer Model 7 Differential Scanning Calorimeter (DSC). Perkin Elmer Diamond DSC is a power compensated DSC which measures the power required to keep the reference pan at the same temperature as the sample pan. The instrument consist of two aluminum pans, one containing sample and other used as reference placed in a holder above the furnace. Temperature range for the instrument is from 700 to -50^{o} C and monitoring is done using thermocouples. For samples that may have glass transition temperatures below room temperature, there is an Intracooler 2 which can achieve temperature down to -50^{o} C. There is a Nitrogen gas cylinder for purging. The Pyris software analyses the plots and helps in calculation of the transition temperatures [36].

About 3-5 mg of sample was used in all tests. The sample was sealed in an aluminum pan and depending on the sample geometry (pellet or powder/flakes) either a volatile or non-

volatile pan was used for sampling. The instrument was calibrated before each set of scans with Indium or Tin, depending on the temperature range of interest. Nitrogen was used as the purge gas to provide an inert atmosphere and to prevent sample degradation. The procedure that was employed for DSC scanning of all the PET samples is described as follows:

- Hold the sample for at 25° C for 1 minute
- Heat the sample from 25 to 280° C at 20° C/minute
- Hold the sample in the melt for 10 minutes
- Cool the sample from 280 to 25° C at 50° C/minute
- Hold it at 25° C for 1 minute
- Heat the sample from 25 to 280° C at 20° C/minute

All DSC thermograms were analyzed using Pyris software for quantitative evaluation of glass transition, crystallization, and melting.

2.2.4 Film Preparation

PET films were prepared by a melt pressing method. The polymer was heated to 260^{o} C in a Carver Melt Press and a pressure of 1000 psi was applied when the polymer was completely melted. Holding time for the polymer in its molten state depended on its geometry (pellets/flakes). Once the film was pressed it was immediately quenched into ice water in order to prevent any crystallization; thus, maintaining the same level of crystallinity between the asr-and self-nucleated nuc-PET samples, which was confirmed by DSC results of the respective films. Both PET films were ~100 μm thick, as determined with a hand-held digital Vernier caliper.

2.2.5 Density Measurements

The densities of asr- and nuc-PET films were measured by floatation using toluene (T) and carbon tetrachloride (CT) solvents, which have densities of 0.8668 and 1.594 g/cm^3, respectively, that are lower and higher than the density of PET. Small pieces of both asr- and p-PET films were placed in a known volume of carbon tetrachloride, vol(CT) containing a magnetic stir-bar, where they floated and then sealed with aluminum foil. The toluene solvent was slowly added from a burette with stirring until each PET film was suspended in the solvent mixture, and the volume of added toluene, vol(T), was noted. The PET densities were then obtained from:

$$\rho_{exp} = \frac{[vol(T)x\rho(T) + vol(CT)x\rho(CT)]}{vol(T) + vol(CT)},$$

2.2.6 Nano-indentation

Nano-indentation is a non-destructive technique for measuring the mechanical properties of polymeric surfaces. It makes use of a probe or an indenter whose mechanical properties are known. The test mode employed was a quasi-static nano-indentation mode in order to measure the hardness and young's modulus of the films.

Nano-indentation was performed on the PET samples using a Hysitron TriboIndenter instrument and the data was analyzed with the TriboScan software. All tests were performed at ambient temperature (approximately 25˚ C). Each of the sample films was indented 5 times in a square pattern using a Berkovich diamond tip. The samples were tested in constant force mode, where a known force is applied on the surface of the film using the indenter and the resultant displacement is calculated in nanometers. A typical topographic view of a nano-indented sample is displayed in Figure 11 [37]. Reduced Young's modulus and hardness

values were all determined automatically by the software. The software helps in the automatic scanning of the surface of the film by adjusting the tip height based on the force feedback and mapping surface topography.

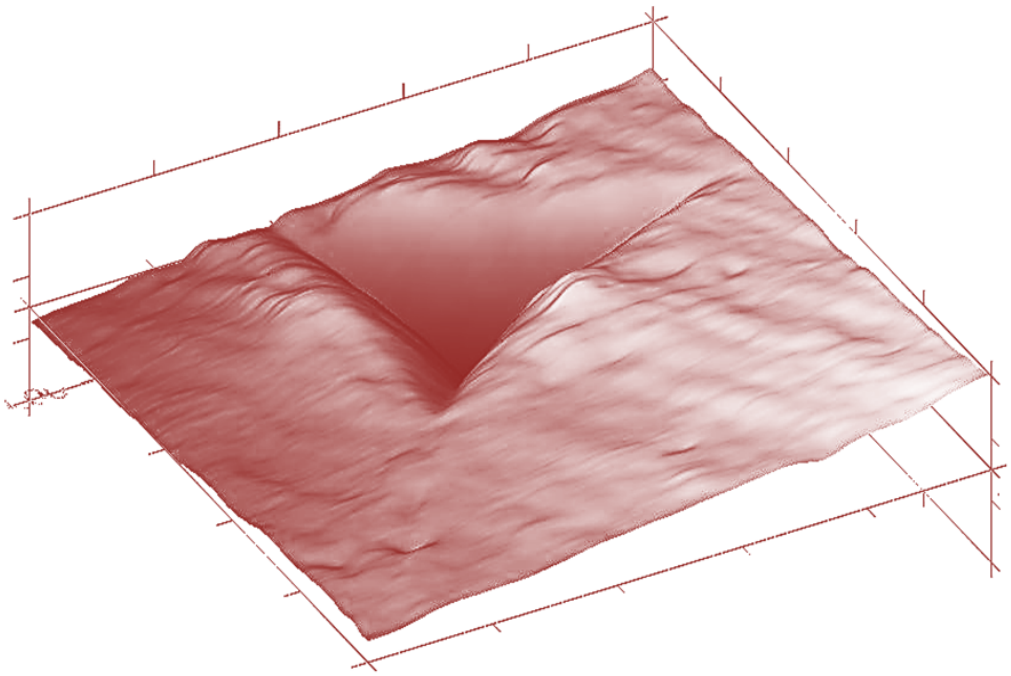

Figure 11: Topographic view of sample after indentation

2.2.7 Polarized Optical Microscopy (POM)

Polarized Optical Microscopy (POM) was used to observe the crystal size and distribution in the quenched PET films. This technique involves passing polarized light through the sample under magnification so that the resultant image is visible to the human eye. The micrographs of asr-PET and nuc-PET films were obtained using a Nikon Eclipse 50i POL Optical Microscope at 100x zoom and the images were captured by a CCID-IRIS/RGB color video camera made by Sony Corp.

2.2.8 Gas Permeability Tests

The CO_2 sorption measurements were made with an ISOSORP®GAS High Pressure Gravimetric Analyzer with an attached Rubotherm Magnetic Suspension Balance assembly. The most important part of this equipment is the Magnetic suspension balance which facilitates accurate weight measurement of the samples. The instrument broadly consists of the Rubotherm magnetic suspension balance connected to the gas tank and vacuum system through a series of valves. The instrument is operated using the MesPro software which enables us to perform blank runs and collection of actual gas permeability data. A simple schematic diagram for the Rubotherm magnetic suspension balance is shown in Figure 12.

The magnetic suspension balance consists of a sample cell that has a small basket in which a V-shape sample is mounted. The sample basket contains magnets and this assembly is connected to a magnetic balance that allows weight measurements. There are four important valves and three of them are shown in Figure 12. Valve 2 and valve 3 are for the gas inlet and vent, respectively, while valve 4 is connected to the vacuum. There is an additional valve 1 which is not usually used. Its function is to vent the system in case there is over pressure in the line and also to provide gas to the sample cell from any tank in the gas cabinet. The setup is quite sturdy and is connected to an electronic display which helps in monitoring the pressure in the cell along with the data collection process (Zero-point to mass point 1 measurements).

The V-shape film samples are placed in the sample basket, which is mounted on a hook connected to the suspension balance. The sample cell was then closed, the gas line was

connected to the Helium tank and vacuum was pulled through the system for about 6 hours. After this a blank run was performed using Helium gas to accurately measure the mass and

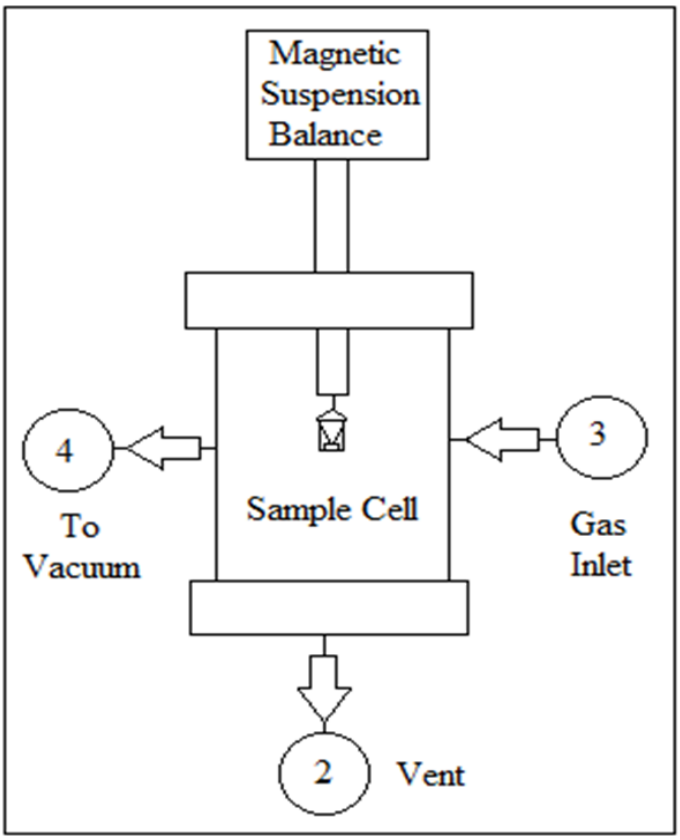

Figure 12: Schematic of the Magnetic Suspension Balance

volume of the sample following which the gas line was connected to the CO_2 tank and the assembly was subjected to vacuum for another 6 hours. Then a CO_2 run was performed on the sample at approximately 21^{o} C and at 2 bar pressure and mass difference curve as a function of time was obtained. A blank run was performed on the empty basket in order to get its mass accurately. MesPro software was used to control the blank and CO_2 runs.

The data were fitted to a permeability model using Kaleidagraph software and the solubility, diffusivity, and permeability values were calculated.

CHAPTER 3: RESULTS AND DISCUSSION

3.1 FTIR Analysis of As-received and Precipitated PET

FTIR spectra were obtained for asr-PET and p-PET. The spectrum of p-PET is nearly identical to that of asr-PET and this tells us that there is no difference in the chemical nature of both PETs and that the method of precipitation is just a physical processes. Figure 13 presents the spectra for asr-PET and p-PET respectively.

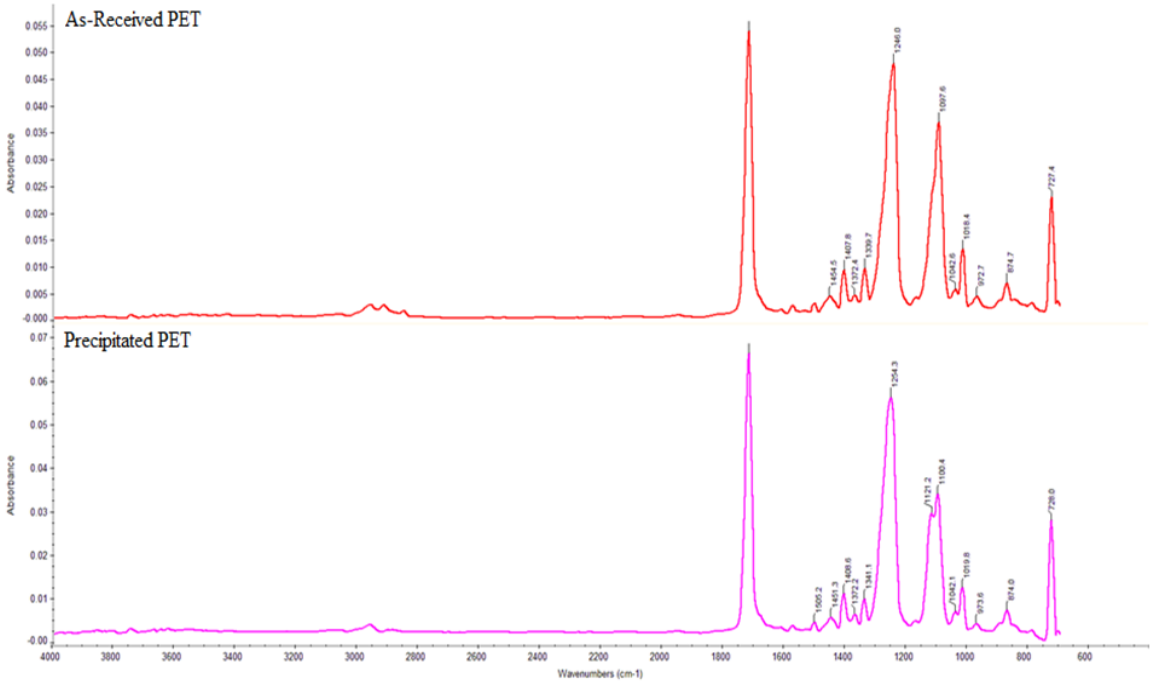

Figure 13: FTIR spectra for asr-PET and p-PET

Although the FTIR spectra for both PETs appear largely identical, a careful examination of the spectra tells us that the peaks in the spectrum of p-PET are more highly resolved which could be because of higher crystallinity and better order in the non-crystalline regions of p-PET.

3.2 Thermal behavior of As-received and Precipitated PET

Thermal behaviors of both asr-PET and p-PET were analyzed using DSC. The test conditions were the same for both samples and have been mentioned in section 2.2.2. The behavior of any sample in the first heating cycle of the DSC scan is the result of its prior processing history. The first rapid cooling cycle from the polymer melt and the subsequent heating cycle demonstrate the actual thermal behavior of PET. Hence, all DSC scans show the first cooling and second heating cycles for the samples. Figure 14 shows the DSC scans for asr-PET.

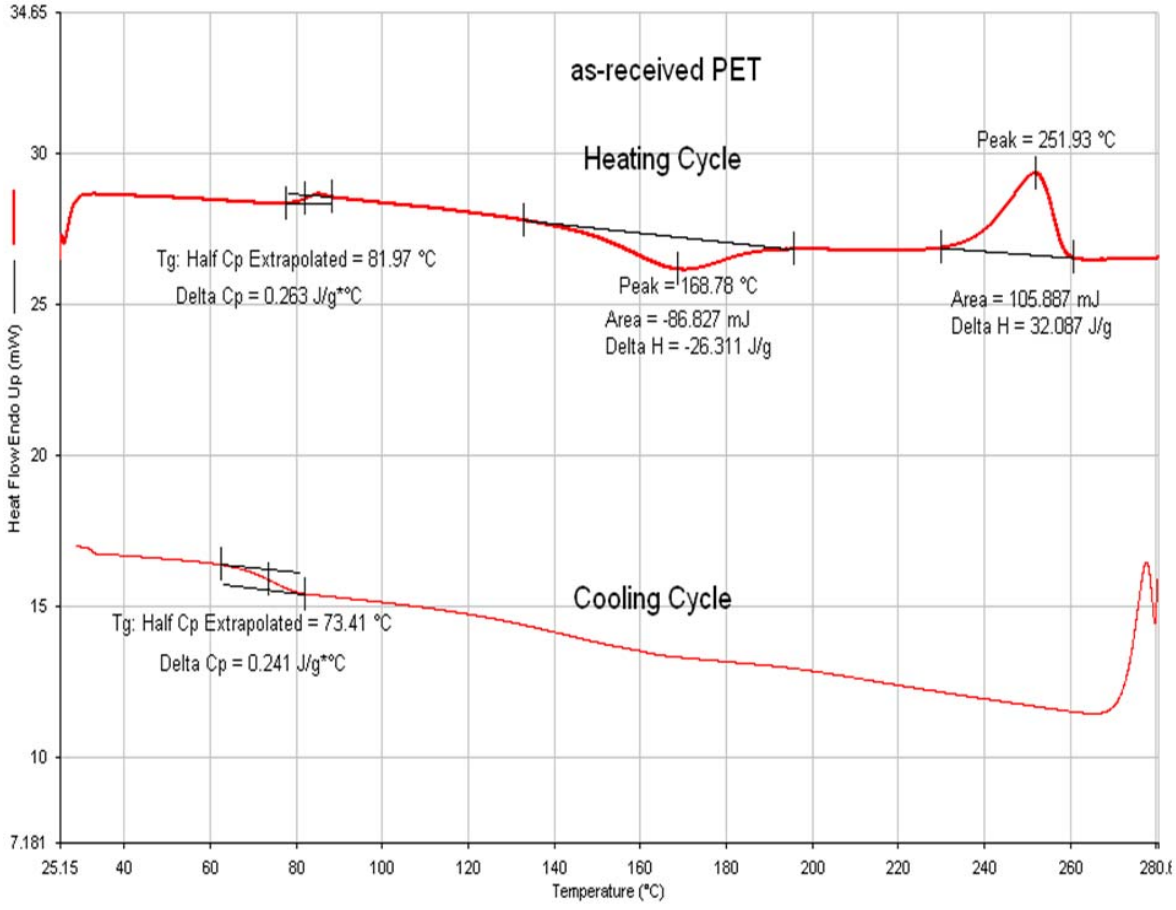

Figure 14: DSC scans for asr-PET

After the first heating cycle the polymer was held in its melt for a substantial time (10 min) to remove its processing history. As we follow the cooling profile of asr-PET when rapidly cooled from its melt, it can be seen that the polymer does not readily crystallize and shows a glass transition suggesting that it has been quenched into a largely amorphous material. The second heating cycle demonstrates a typical trend for largely amorphous PET, where the polymer evidences glass transition, crystallization, and a melting.

Figure 15 illustrates the DSC scans for p-PET. The polymer is initially heated past its melting point and was held in the melt for 10 min. When p-PET is rapidly cooled from its

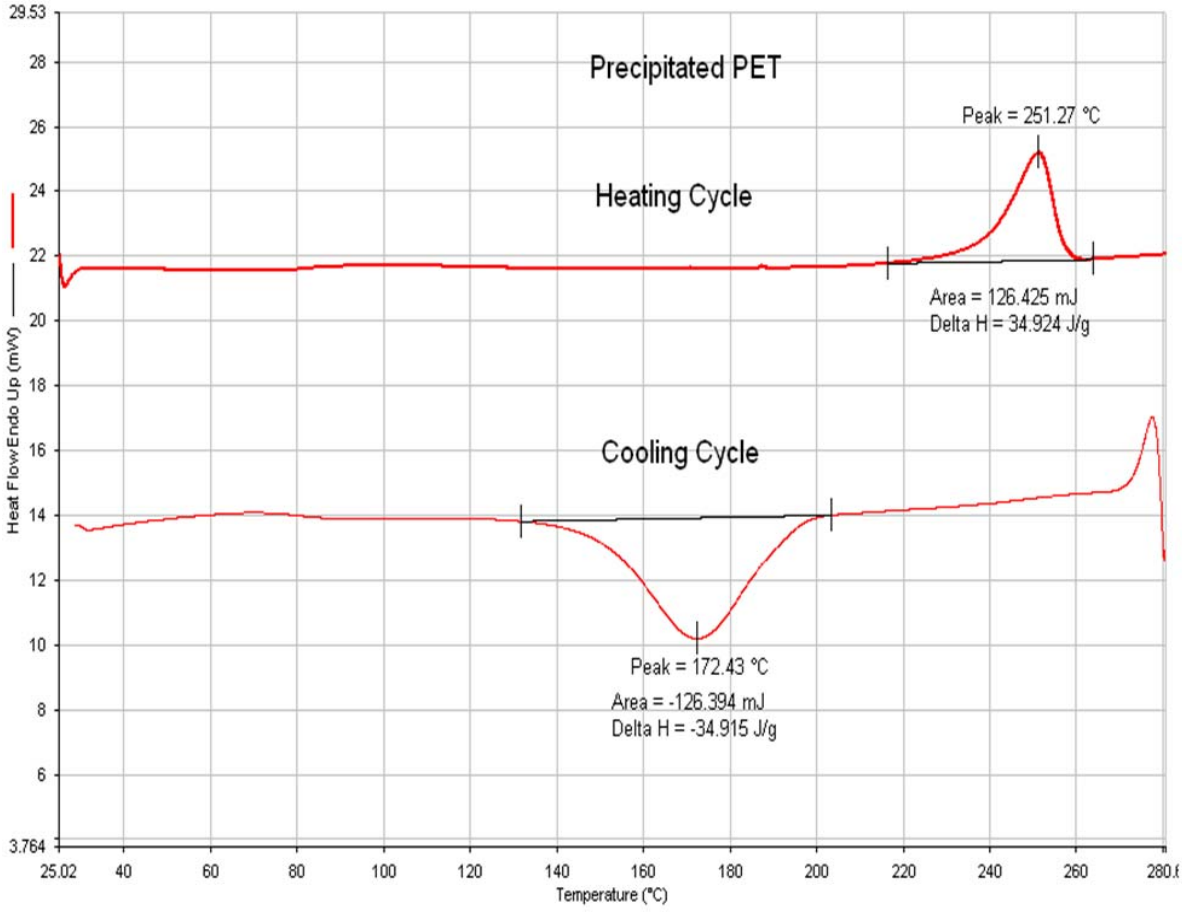

Figure 15: DSC scans for p-PET

melt it shows a crystallization peak suggesting that p-PET crystallizes more readily and rapidly than asr-PET. In the following heating cycle p-PET neither shows a glass transition nor crystallization, but only exhibits a melting endotherm, which suggests that the thermal behavior of p-PET is quite distinct from that of asr-PET. Table 6 summarizes the DSC results for asr-PET and p-PET.

Table 6: DSC data for as-received and precipitated PETs

Sample	Cooling Cycle			Heating Cycle					% Crystallinity
	T_g (^oC)	T_c (^oC)	ΔH_c (J/g)	T_g (^oC)	T_c (^oC)	ΔH_c (J/g)	T_m (^oC)	ΔH_m (J/g)	(X_c)
asr-PET	73.4	-	-	81.9	168.7	-26.3	251.9	32.0	4.1
p-PET	-	172.4	-34.9	-	-	-	251.27	34.9	24.9

Percent crystallinity has been calculated using the data from the heating cycle for both asr-and p-PET from the following equation, where $\Delta H_m^o = 140$ J/g [9].

$$\% \text{ Crystallinity } (X_c) = (\Delta H_m - \Delta H_c) \times 100/\Delta H_m^o$$

The DSC thermograms for p- and asr-PET are distinctly different from each other. During their cooling scans from the melt it can be clearly observed that asr-PET can be quenched into a largely amorphous material, which demonstrates its slow crystallizing nature. On the other hand, p-PET shows a crystallization peak virtually identical in magnitude to its subsequent melting peak, indicating that even on cooling p-PET at a high rate the polymer crystallizes rapidly. The effect of this difference in their crystallization rates during cooling is evident in the subsequent heating cycles for asr- and p-PET's. The heating cycle for asr-PET shows a glass transition due to its largely amorphous morphology and the crystallinity observed during melting is primarily induced during subsequent heating above the glass-transition, which implies that asr-PET cooled rapidly from its melt has very low crystallinity.

In the heating cycle, absence of the glass transition and crystallization in the p-PET thermogram indicates that the non-crystalline regions in p-PET are organized differently than in asr-PET. The glass transition phenomenon is related to the amorphous segments of the polymer and its absence in p-PET indicates better orientation, tighter packing of its chains in the non-crystalline domains. The values of the crystallization exotherm during cooling and melting endotherm during heating cycles for p-PET are almost the same, which tells us that the polymer crystallizes completely during its rapid cooling. p-PET was subjected to repeated heating and cooling cycles, but its thermal behavior remained unchanged thus confirming that thermal recycling and holding the polymer in the melt has not removed the structural reorganization achieved by precipitating PET.

The fast crystallizing nature of p-PET can be attributed to the change in its conformation within the non-crystalline domains as a result of its processing via the precipitation technique.

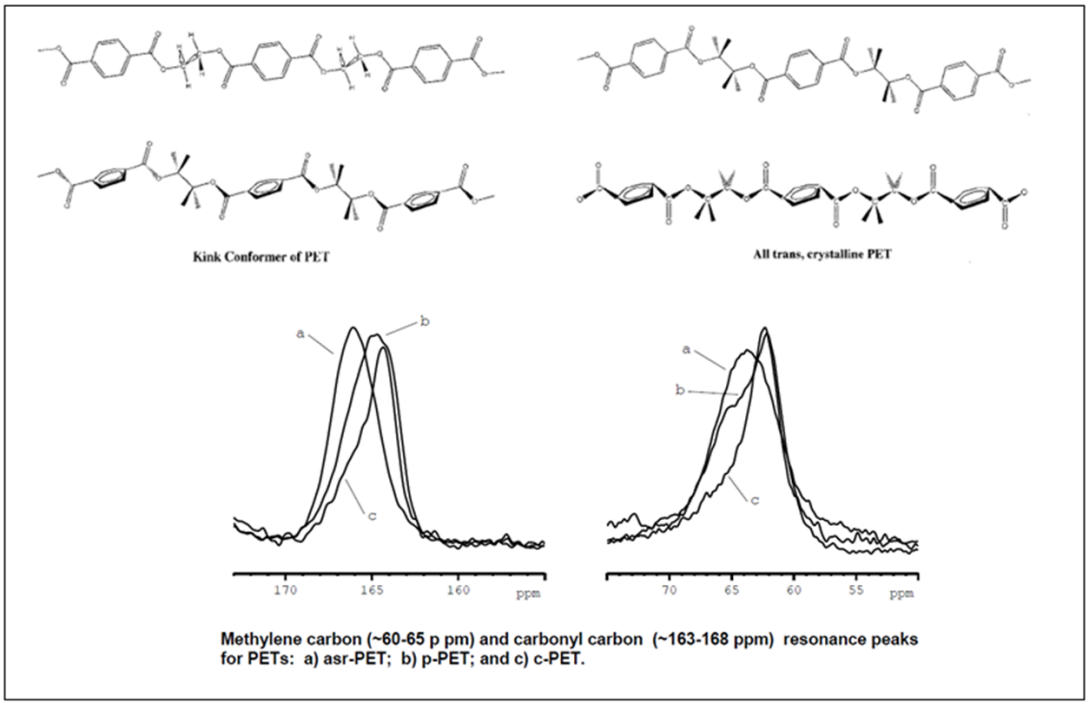

Figure 16: Conformational changes in PET

Figure 16 shows the kink and all trans-crystalline conformers for PET. In a random coil configuration, the ethylene glycol -CH2 – CH2- bonds in PET are predominantly gauche. For the random coil to transform into the all trans-crystalline conformer, large segments of the polymer chains are required to rotate making it highly improbable. When PET is processed with γ-CD, the included chains assume a gauche-trans-gauche ethylene glycol kink conformation. The ability of c-PET to crystallize rapidly is dependent on the inter conversion of its ethylene glycol fragments with gauche-trans-gauche kink conformations to the all trans-crystalline conformation made facile by counter rotations about the - CH2 – O- and

-O – CH2- bonds, which do not require much "swept-out" volume. NMR spectra of c-PET and p-PET show similar chemical shifts which are distinct from that of asr-PET, suggesting that p-PET also assumes a kink conformation thus making it a fast crystallizing polymer [27].

3.3 Thermal Behavior of Self-Nucleated PET and Its Nucleation Mechanism

The thermal behavior of asr-PET nucleated with 5 wt% p-PET (nuc-PET) was found to be quite similar to that of p-PET (See Figure 17). When rapidly cooled after spending substantial time in the melt, nuc-PET is found to crystallize rapidly. It develops its entire crystallinity during the cooling cycle much like p-PET, thus also behaving like a fast crystallizing polymer. In the subsequent heating cycle, nuc-PET does not evidence a glass

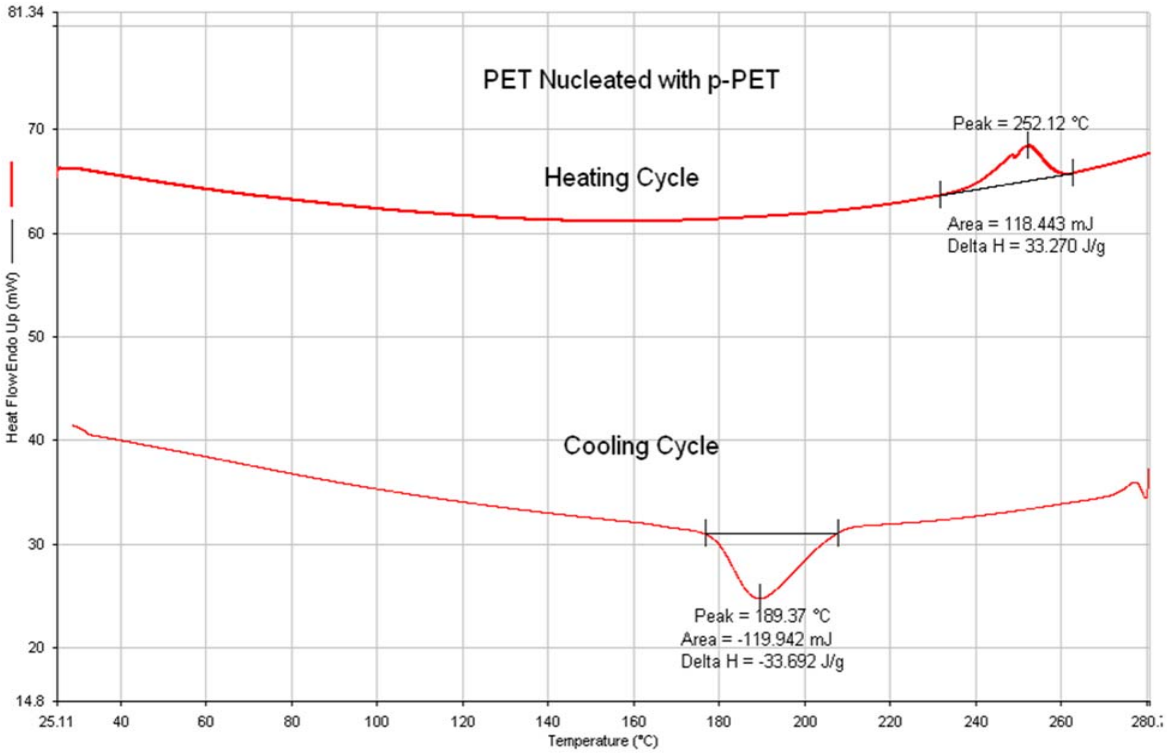

Figure 17: DSC scans for Self-Nucleated PET

transition or crystallization, but only melting. The crystallinity developed in nuc-PET is much larger than that in asr-PET and is comparable to the crystallinity observed in p-PET.

It is interesting to observe that as little as 5% of p-PET can influence the behavior of the remaining 95% of asr-PET. The explanation for this lies in the mechanism by which p-PET nucleates and controls the morphology of the self-nucleated material. Figure 18 suggests this nucleation mechanism.

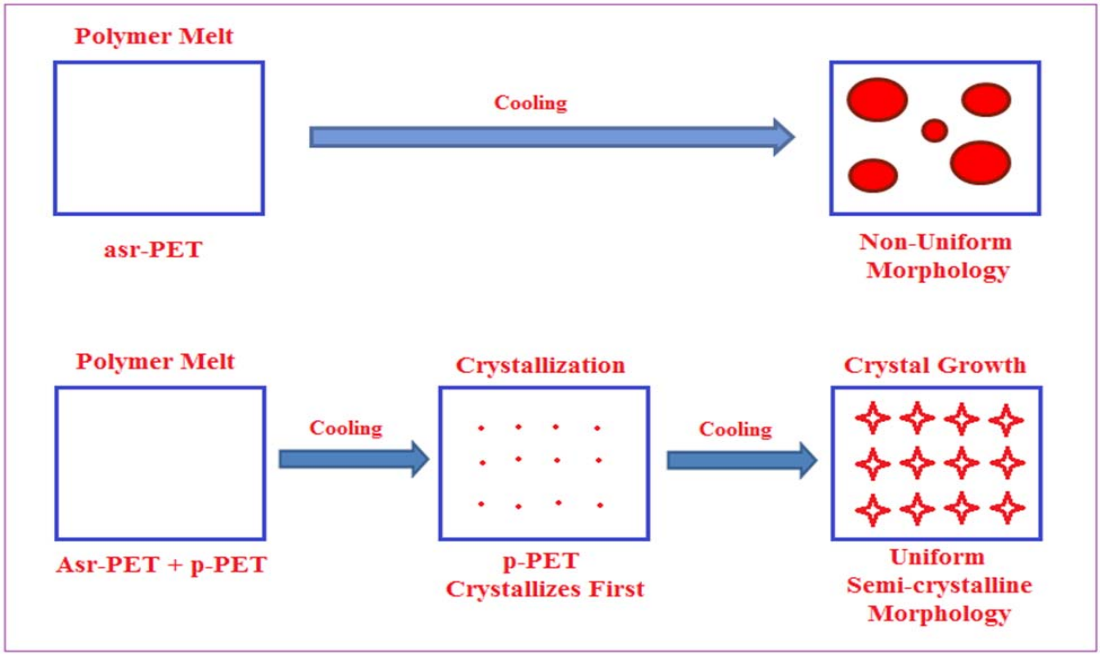

Figure 18: Mechanism of Self-Nucleation in 5:95 p-PET:asr-PET to form nuc-PET

From the thermal behavior it is clear that p-PET crystallizes even when cooled at a high cooling rate making it a fast crystallizer, while asr-PET is a slow crystallizer. When we follow the cooling profile from the polymer melt, asr-PET does not crystallize due to its slow crystallizing nature and the resultant polymer has low crystallinity and non-uniform morphology.

When we mix a small amount of p-PET with asr-PET and subject the polymer mixture to melting conditions, asr-PET loses its processing history and goes back to random coil configurations, whereas p-PET retains its extended chain conformations. On cooling this mixture from its melt at a rate where asr-PET hardly crystallizes, p-PET rapidly crystallizes and the domains where p-PET is present in the mixture crystallize first and provides nucleation sites. These active sites shorten the induction time and enhance the rate of crystallization from the molten phase. They also lower the free energy barrier for stable nucleus formation and initiate simultaneous spherulite growth. Formation of nucleation sites can be referred to as primary crystallization which is followed by secondary crystallization, wherein crystal growth is continued from these nucleation sites resulting in a uniform semi-crystalline morphology.

We have observed that asr-PET nucleated with 2 wt% p-PET also produces a nuc-PET that is repeatedly and rapidly crystallizable from its melt.

3.4 Evaluation of Self-Nucleation: p-PET vs. Traditional nucleating agents

p-PET is as an effective nucleating agent, and it is important to compare its nucleating ability with some of the common nucleating agents. For this purpose asr-PET was nucleated with γ-CD, talc, and glass particles, and the resultant DSC behaviors were observed. These nucleating agents are insoluble in the polymer melt and hence follow a heterogeneous mode of nucleation, unlike p-PET which follows a homogeneous nucleation. Figure 19 shows the thermal behavior of asr-PET nucleated with the above nucleating agents. All the thermograms represent first cooling and second heating cycles. From the thermogram of asr-PET nucleated with γ-cyclodextrin it is clear that nucleation is limited and the behavior is

similar to asr-PET. The thermogram of 30% glass reinforced PET is similar to that of self-nucleated PET, but it is important to note that the amount of the glass reinforcement/nucleant

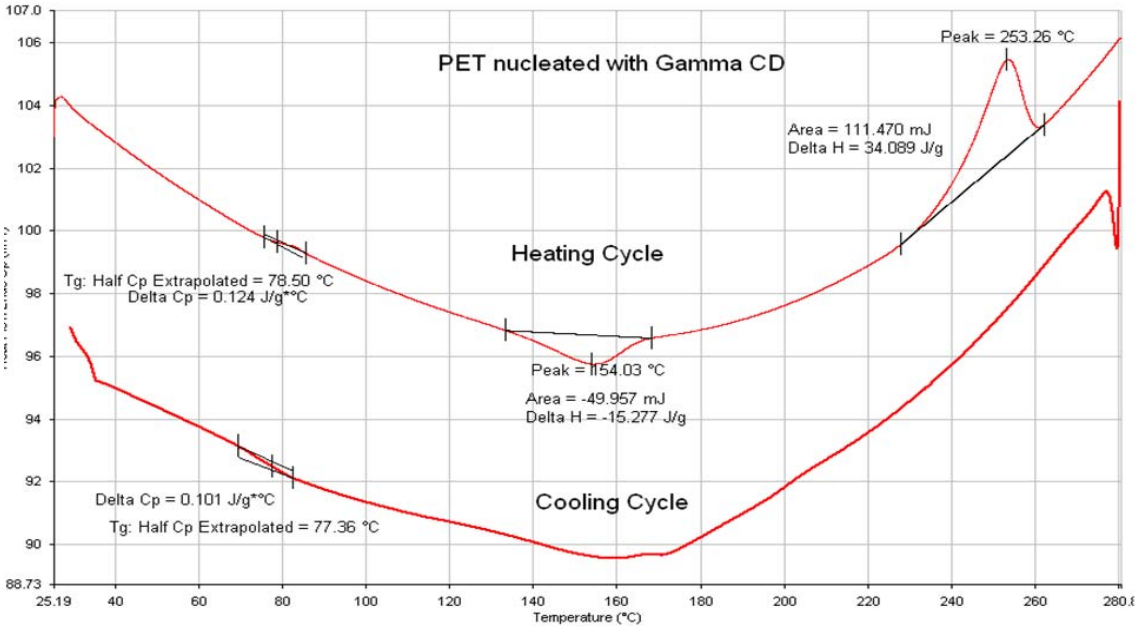

a)

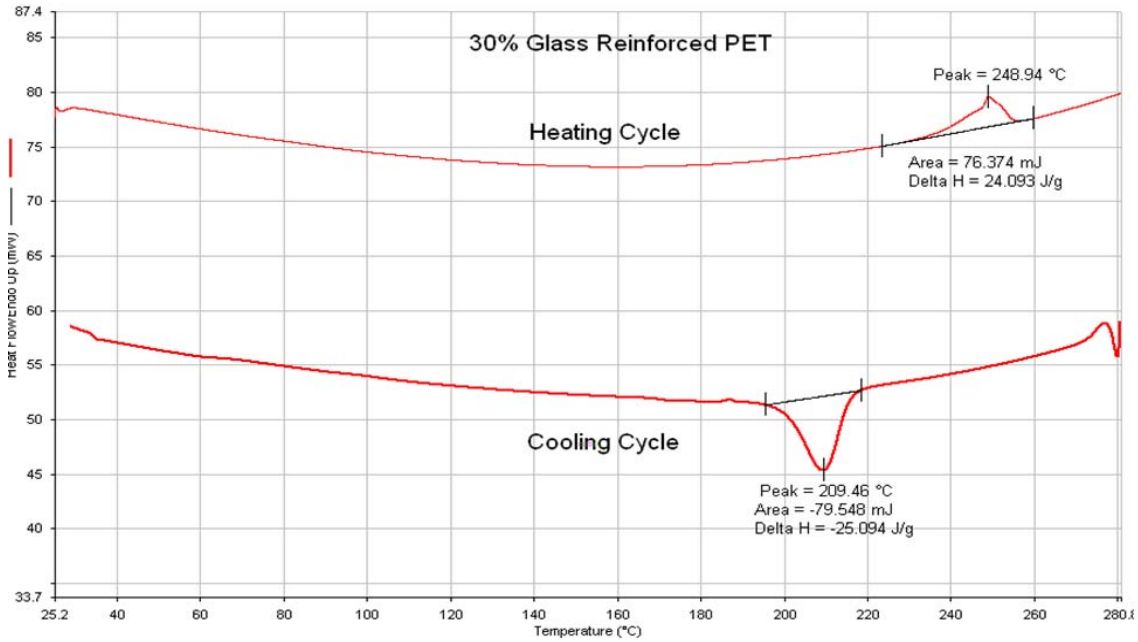

b)

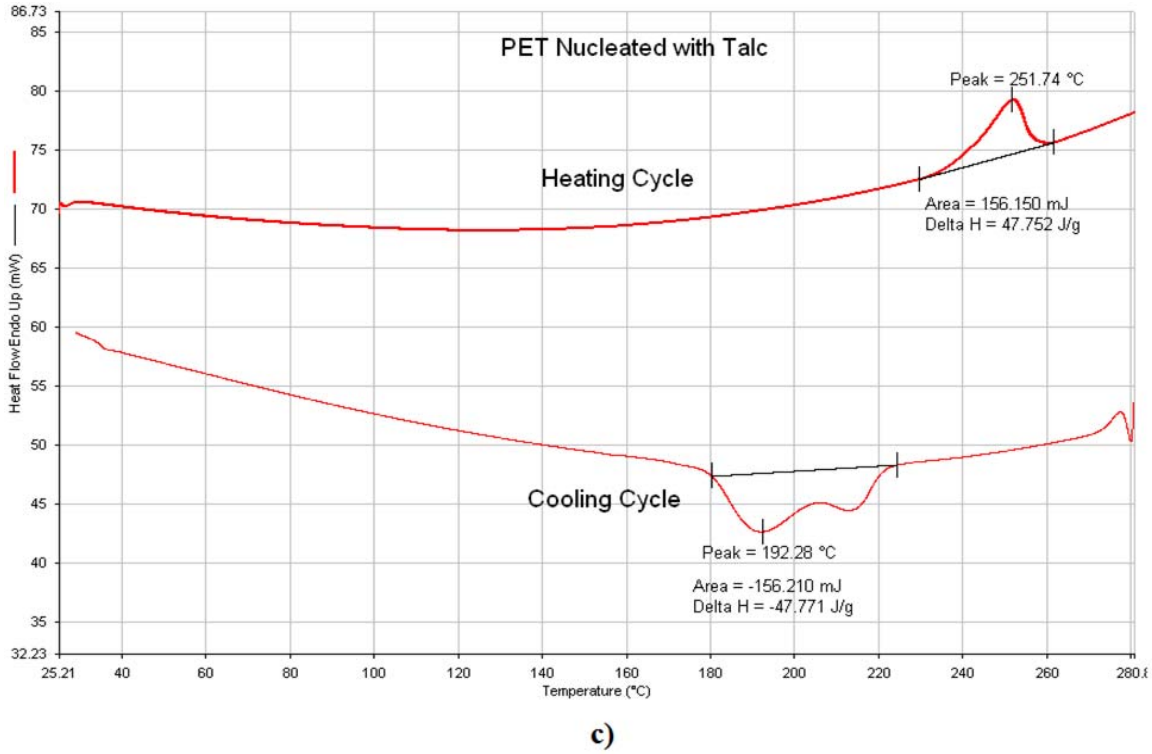

c)

Figure 19: DSC thermograms of PET nucleated with a) 5% γ-cyclodextrin, b) 30% glass particles and c) 5% talc

in this commercially available PET is quite high, when compared to the amount of p-PET added in self-nucleated PET. Talc shows the best nucleation behavior yielding a higher heat of crystallization during the cooling cycle.

The crystallization endotherm in PET nucleated with talc is broad and suggests that even if there is more crystallinity, the crystal sizes may be largely non-uniform in size and distribution. Percent crystallinity in each of the nucleated polymers was calculated from their respective thermograms and Figure 20 compares the nucleating efficiency of each of the nucleating agents.

PET nucleated with γ-cyclodextrin has low crystallinity and hence γ-cyclodextrin is not as efficient as the other nucleants. The 30% glass reinforced PET commercial sample has lower crystallinity than self-nucleated PET, while PET nucleated with Talc show a higher %

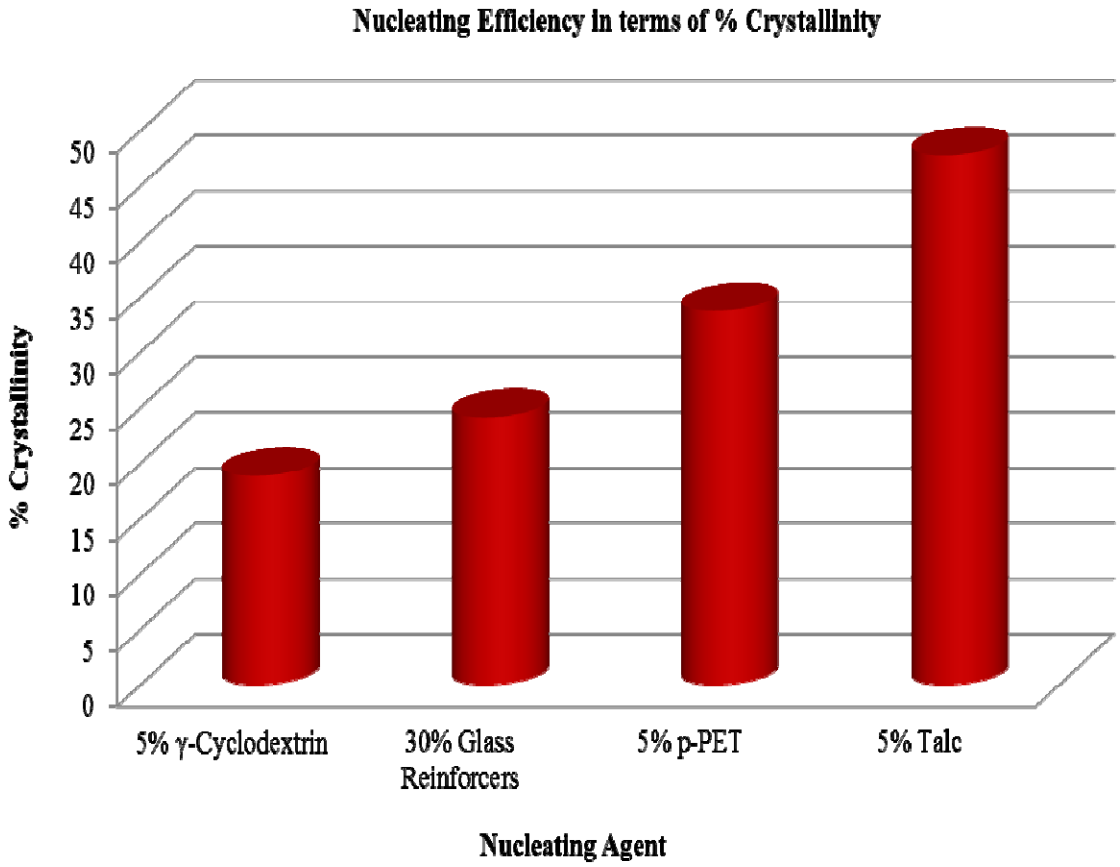

Figure 20: Percentage crystallinity in asr-PET nucleated with different nucleants

crystallinity than self-nucleated PET. In this comparison the physical size of the nucleants has not been taken into consideration, and talc could have more effectively nucleated PET than the other nucleants owing to its much finer granular size [38]. Thus when compared with traditional nucleants, p-PET shows comparable, and in most cases, better nucleating ability and so it is interesting to evaluate the properties of self-nucleated PET.

3.5 PET Densities.

The quenched asr- and nuc-PET films are clear in appearance. DSC scans of the two films are shown in Figure 21 and these represent the first heating cycle. The DSC results suggest that both asr- and nuc-PET films have the same level of crystallinity, but a careful

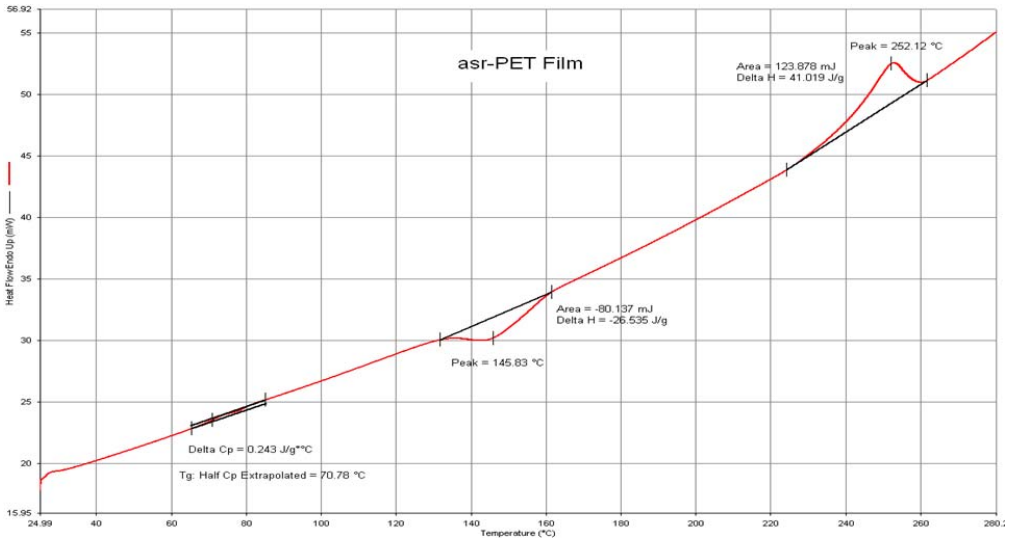

a) asr-PET Film

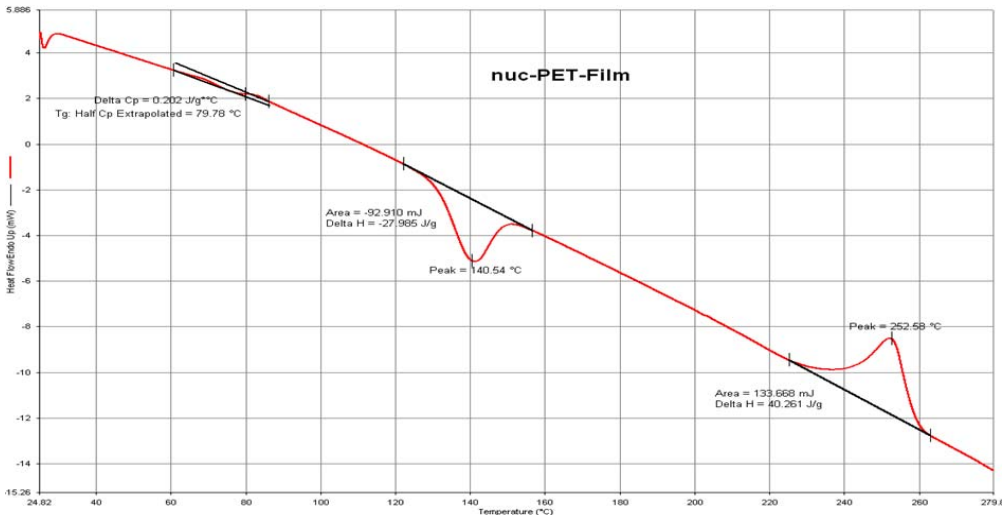

b) nuc-PET Film

Figure 21: DSC Heating Scans for a) asr-PET and b) nuc-PET

observation of their crystallization curves tells us that there is some difference in their structural organizations or morphologies. This is also clear from the slight difference in their glass transition temperatures, where T_g of nuc-PET is higher than that of asr-PET, suggesting that there is more order in the amorphous domains of the nuc-PET.

Percentage crystallinity in each of the films was calculated from their respective thermograms and was found to be $X_c \sim 10\%$. The densities of these films were obtained using the flotation technique and the results are summarized in Table 7.

Table 7: Densities of asr-PET and nuc-PET

Sample	Density at 25° C (g/cm^3)
asr-PET	1.368
nuc-PET	1.386

The higher density of the nuc-PET film (~ 1.8% higher) with the same low level of crystallinity as in the asr-PET film can be attributed to the higher orientation and increased order and packing of chains in its amorphous domains, which is seen even after the polymer film was quenched from the melt into ice water. This shows that nuc-PET has a tendency to organize differently than asr-PET even when melt quenched at very high cooling rates.

3.6 Nano-Indentation of PET Films

Nano-indentation provides a quantitative technique to evaluate near surface mechanical properties of thin films with the help of its depth sensing capability. This is accomplished with the help of a diamond indenter with a well-defined tip [41]. The instrument when operated in a quasi-static mode helps us in evaluating the hardness and Young's modulus for the films. Figure 22 illustrates a typical loading and unloading curve for the asr-PET film sample.

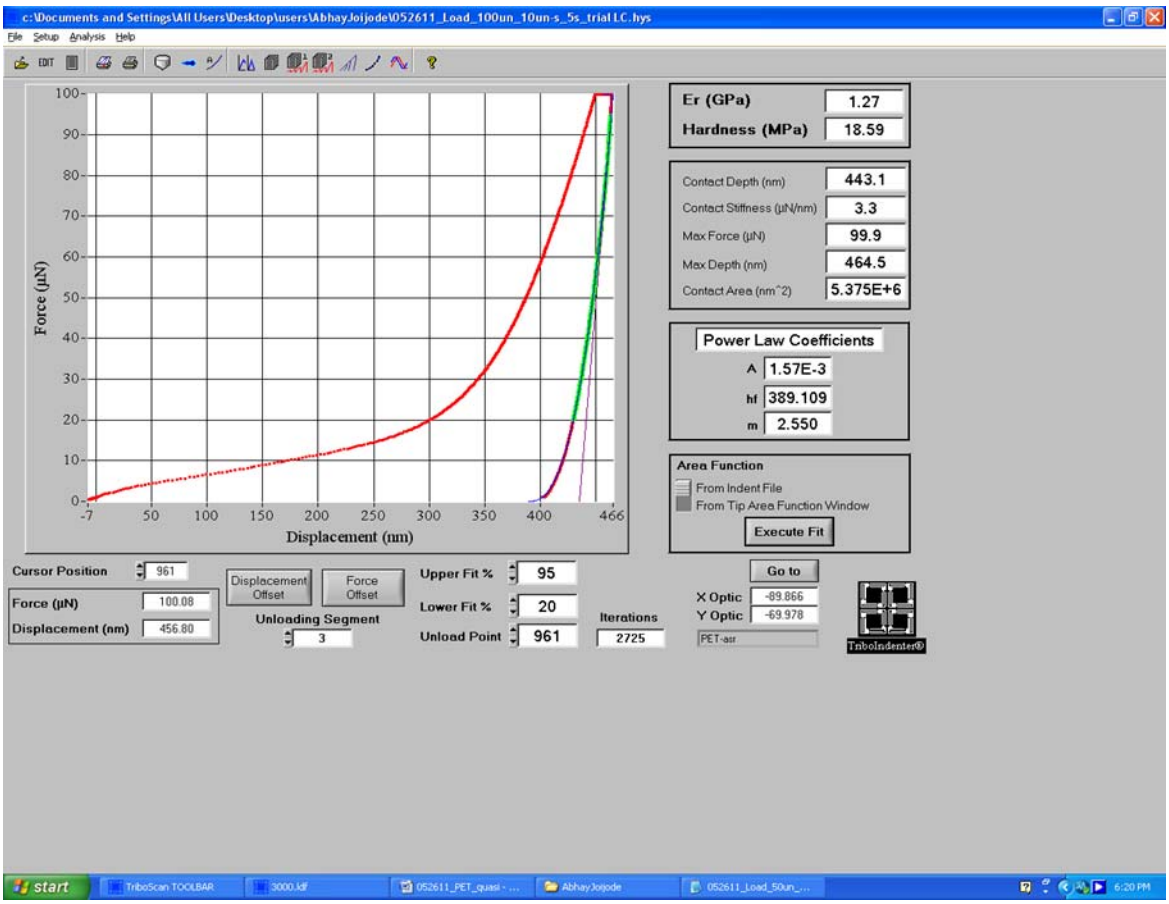

Figure 22: Loading-unloading nano-indentation curve for asr-PET sample

The software calculates the reduced young's modulus and the hardness values. The following equation helps us in calculating the actual young's modulus from the reduced Young's modulus data obtained from the software,

$$\frac{1}{E_r} = \frac{(1-\upsilon_i^2)}{E_i} - \frac{(1-\upsilon_s^2)}{E_s}$$

where,

E_r – Reduced Young's Modulus (GPa)

E_i – Elastic Modulus of the Diamond Indenter (GPa)

E_s – Young's Modulus of PET Sample (GPa)

υ_i – Poissons Ratio for Diamond Indenter

υ_s – Poissons Ratio for PET Sample

The elastic modulus and poisons ratio for the diamond indenter are 1140 GPa and 0.07 respectively [40], while the poisons ratio for largely amorphous PET is 0.37 [41]. Figure 23 summarizes the results for Hardness and Young's modulus for the PET films, as a function of the applied force.

The values of hardness and Young's modulus obtained for the asr-PET films are comparable to those mentioned in the literature [42, 43]. From the results it is clear that the nuc-PET films have significantly higher hardness and stiffness. The load bearing capacity of nuc-PET is likely higher on account of better alignment of the polymer chains in the predominant amorphous regions, resulting in their closer packing at a higher density.

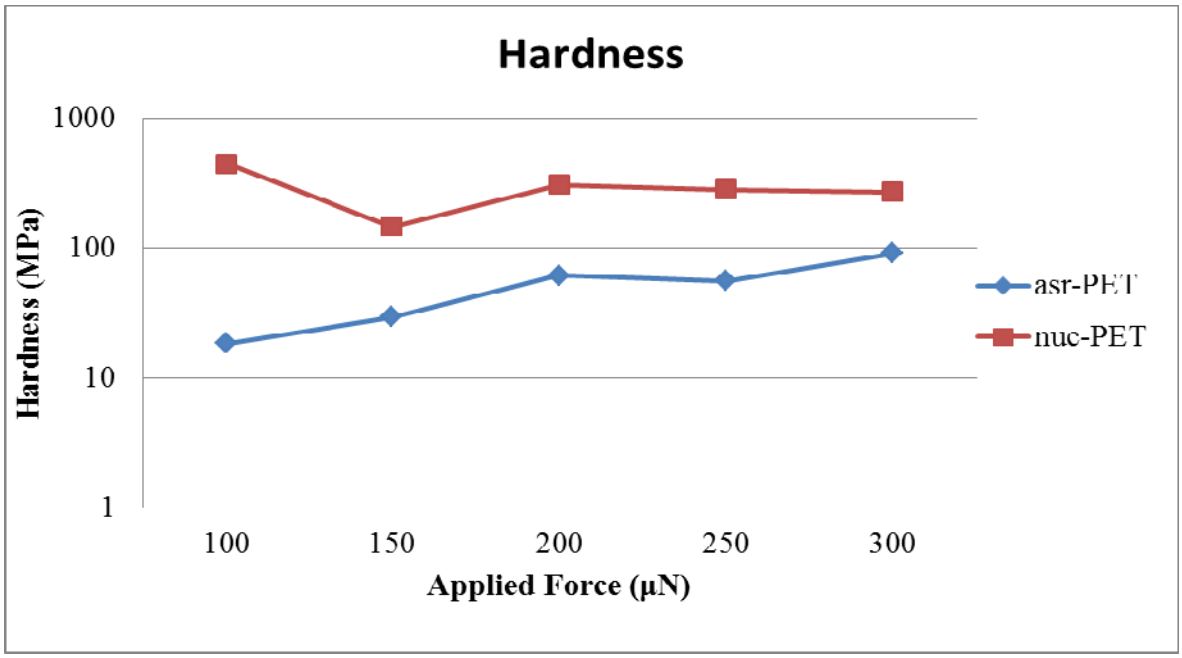

a)

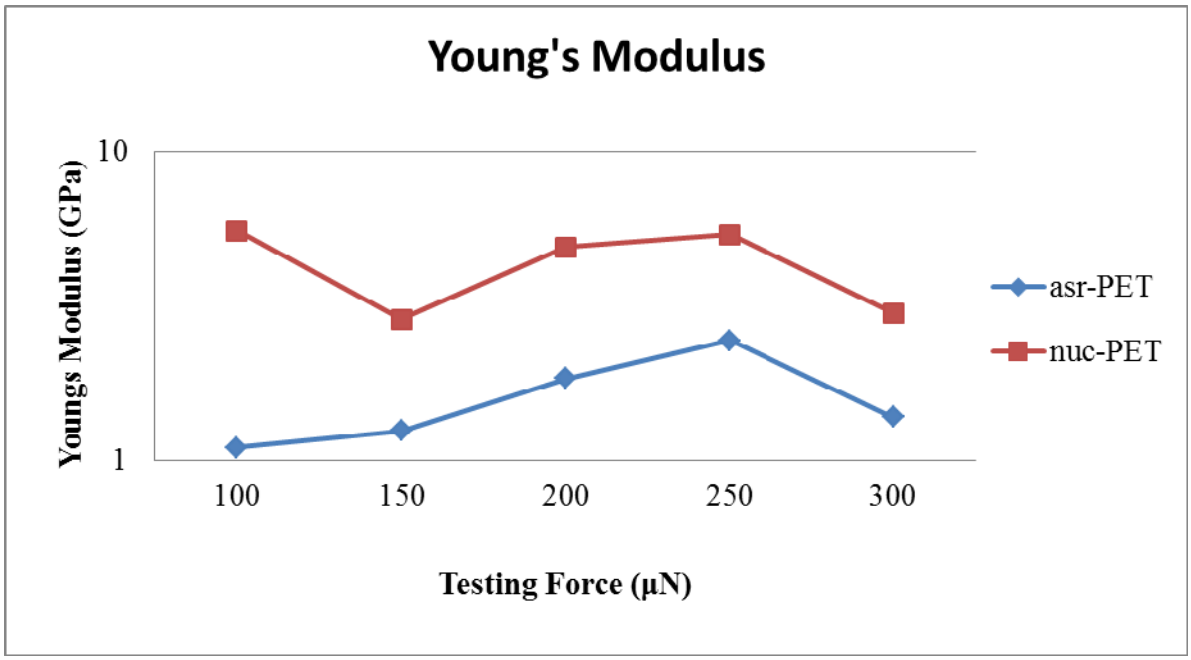

b)

Figure 23: a) Hardness and b) Young's Moduli for asr- and nuc-PET films

3.7 Polarized Optical Microscopy

Polarized optical microscopy images were obtained for asr- and nuc-PET films in order to observe the crystal size and distribution. The polarized optical microscope enables us to view magnified images of the PET films under polarized light and the images are shown in Figure 24.

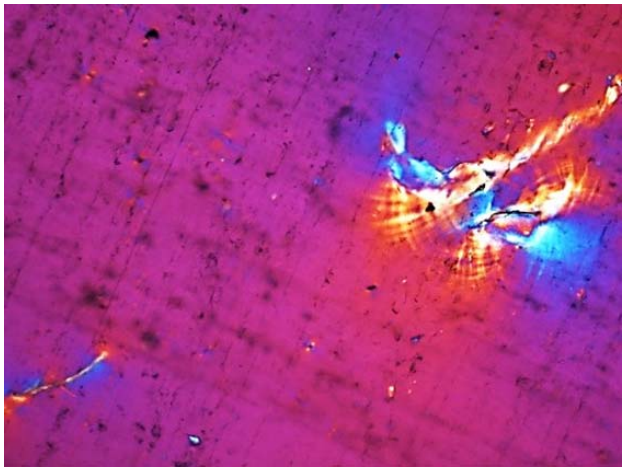

a) asr-PET

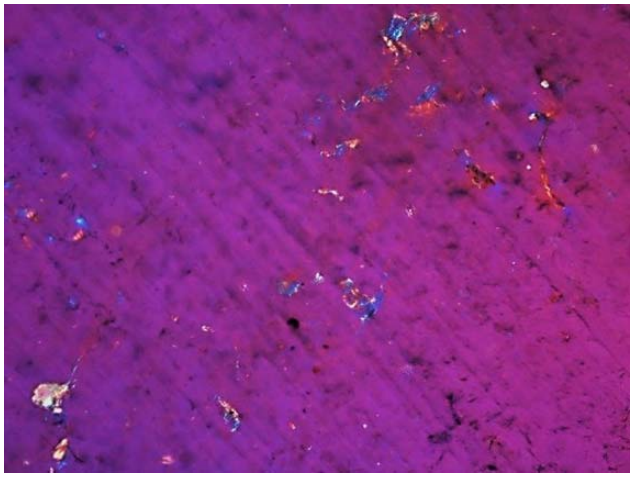

b) nuc-PET

Figure 24: Polarized Optical Micrographs of a) asr-PET and b) nuc-PET

Since the PET films are largely amorphous, very few crystals were observed under the microscope. The micrograph of asr-PET shows non-uniform crystal sizes and distribution, while the micrograph for nuc-PET shows much smaller crystals which are uniformly distributed. These results support our previous discussion of the mechanism of self-nucleation, where the dispersed p-PET controls the semi-crystalline morphology of the resulting nuc-PET.

3.8 Gas Permeability Tests

Impermeability to gases is usually a critical requirement for polymers used as packaging materials. The coefficient of permeability (P) is related to the diffusivity (D) and the solubility (S) of gases in the polymer under study ($P = S \times D$). Diffusivity is associated with the movement of the gas molecules through the cross section of the polymeric film, while solubility corresponds to the amount of gas that gets dissolved in the polymer. During the packaging process the pressure of the gas is usually different than under ambient conditions, so it is important to study the effect of the working pressure on the permeability of the packaging material.

Figure 25 shows the solubility curves for asr- and nuc-PET, while Table 8 summarizes the gas permeability results. The data obtained from the gas permeability test was fitted to a permeability model using the Kaleidagraph software. Solubility and diffusivity values are determined from the solubility curve of the PETs. The value at which the curve flattens (M_∞) is the maximum amount of gas that is absorbed by the sample. Since solubility of the gas is dependent on the pressure (P) at which the experiment is carried out the solubility values are reported as the amount of gas absorbed per unit applied pressure. Diffusivity in PET is

dependent on the slope of the curve (m2) which is shown in Figure 25 and the following equations were used to calculate solubility, diffusivity and permeability in the PET films,

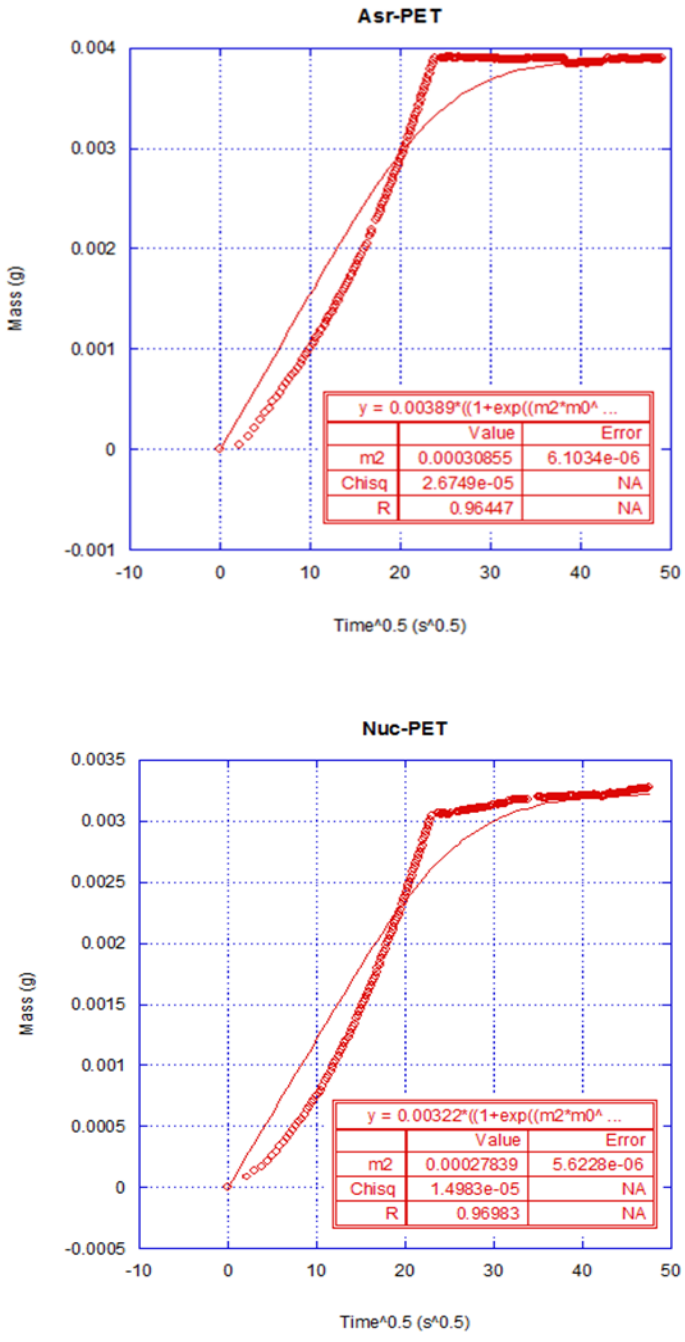

Figure 25: CO_2 absorption curves for asr-PET (above) and nuc-PET (below)

Table 8: CO_2 (0.2MPa) solubility, diffusivity, and permeability in PET films

Polymer Sample	Solubility ($S \times 10^7$) (g [CO2].g^{-1} [sample].Pa^{-1})	Diffusivity ($D \times 10^8$) (cm^2.s^{-1})	Permeability ($P \times 10^{14}$) (cm^2.s^{-1}.Pa^{-1})
asr-PET	6.13	2.68	1.64
nuc-PET	2.38	2.40	0.57

$$S = M_\infty \text{ (g [CO2].g}^{-1} \text{ [sample])} \times (\text{Pressure})^{-1} \text{ (Pa}^{-1}\text{)}$$

$$D = m2 \text{ (s}^{-1}\text{)} \times (\text{Thickness})^2 \text{ (cm}^2\text{)}$$

$$P = S \text{ (Pa}^{-1}\text{)} \times D \text{ (cm}^2\text{.s}^{-1}\text{)}$$

Under ambient conditions, permeability of CO_2 is low in most polymers. However, when the polymers are processed at higher pressures for different applications, the permeability factor becomes critical and needs to be taken in to account. This fact is more evident for polymers used in packaging of carbonated beverages, where they are subjected to pressurized CO_2.

Gas barrier properties are related to the morphology of the polymer. It is influenced by the level of crystallinity, available free volume, and sizes and alignment of the amorphous domains in the polymeric material. In this study the polymer samples are processed in to

films in such a way that all the samples are at the same level of crystallinity, so their resultant gas barrier functionalities are dependent only on the polymer chain alignment and packing in each PET sample.

Solubility of gases in polymers is related to the free volume available for the gas to be absorbed in, while diffusivity is dependent on the crystallinity and chain orientation in the amorphous domains. For our PET films it is clear that CO_2 permeability values are much higher for asr-PET than for nuc-PET. nuc-PET has a much lower CO_2 solubility and only marginally lower diffusivity, possibly due to aligned and more densely packed chains in the amorphous regions that provides a much greater barrier (~3 times that of asr-PET) for the passage of CO_2 molecules through the film. This is in agreement with the proposal that the processing of PET *via* self-nucleation has brought about structural change from a random coil configuration to largely extended-chain morphology. The gas barrier results for PET are consistent with the DSC and density observations. As a result of different arrangements of the polymer chains in the p-PET nucleant, nuc-PET crystallizes more and faster and with more densely packed chains in its amorphous regions than asr-PET, when they are both cooled at the same rate from their melts.

3.9 Repeated Self-Nucleation

Small quantities of p-PET have been demonstrated to act as self-nucleating agents. Now, when we add 5% of nuc-PET to 95% of asr-PET and observe the thermal behavior of the resultant polymer from its DSC scan, it behaves like a fast crystallizing polymer wherein its crystallinity is completely developed during the rapid cooling cycle. Figure 26 illustrates repeated self-nucleation.

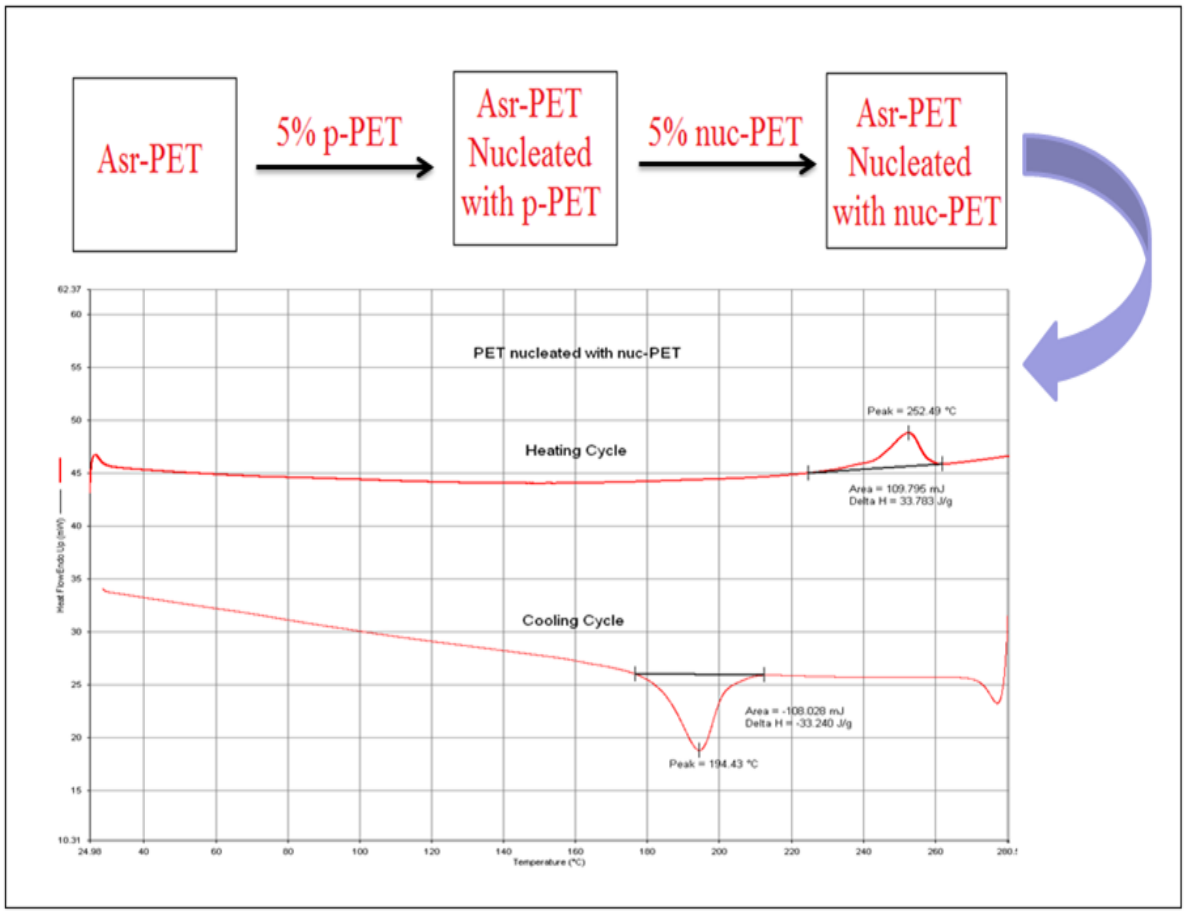

Figure 26: Repeated Self-Nucleation

This behavior can be attributed to the fact that nuc-PET crystallizes rapidly at a higher temperature than that of asr-PET. Due to this, it can control the semicrystalline morphology of PET and can act as a nucleating agent all by itself. If we estimate the amount of p-PET actually present in the repeatedly nucleated PET, it comes out to 0.25%. This significantly reduces the amount of p-PET needed for the self-nucleation process thus making it more efficient and economically viable.

CHAPTER 4: CONCLUSIONS

The structure and morphology of asr-PET samples have been successfully modified *via* the precipitation of PET and its use as a self-nucleant for the melt-crystallization of asr-PET. The resultant materials have been demonstrated to be distinct from the usual melt-processed PET samples. Their experimental analyses have provided ample evidence that p-PET has a distinct thermal behavior in comparison to asr-PET. Furthermore, it does not revert back to random-coiled entangled chain configurations even after repeated melt processing, where it spends substantial time in the melt, and, so, can be successfully used in small quantities as an effective self-nucleating agent.

In addition to different levels of crystallinity, our results indicate that there exists a difference in the structural organizations of the non-crystalline portions of asr- and nuc-PET. Spectroscopic and viscometric observations indicate that these organizational differences are physical in nature and not the result of degradation or cross-linking occurring during the precipitation and nucleation processes. Density measurements confirm the amorphous portions of nuc-PET are denser than the amorphous regions of asr-PET. This is likely because the polymer chains in the amorphous regions of the asr-PET are completely disordered (randomly-coiled and entangled), while in nuc-PET they appear to be at least somewhat extended and less randomly-coiled and entangled. Previous work on the measurement of melt viscosities indicate that p-PET has a lower melt viscosity than the asr-PET, also suggesting that this difference is on account of lesser chain entanglements in p-PET [29].

As a result nuc-PET has been shown to possess better mechanical, thermal, and gas barrier properties, with smaller crystals more homogeneously distributed, i.e., with a semi-crystalline morphology that was controlled by processing (precipitation/nucleation) as indicated in Figure 27. The general conclusion that can be drawn from all these observations is that nuc-PET has a unique structural organization that differs both microscopically and macroscopically from normally processed asr-PET, with distinct non-crystalline regions.

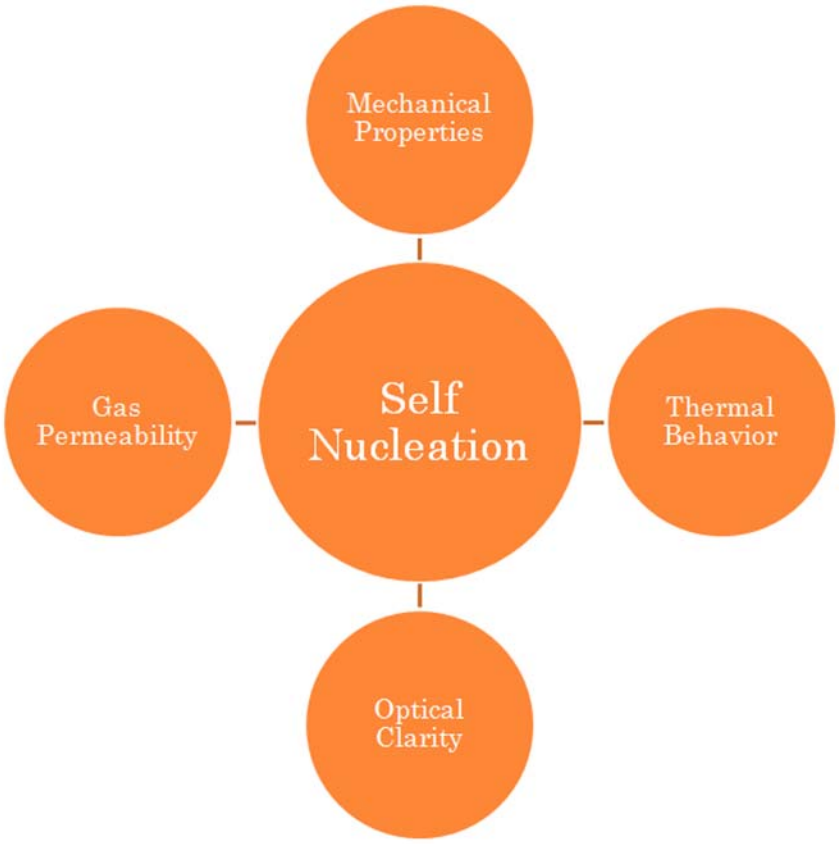

Figure 27: Structure-Property Relationships for nuc-PET

CHAPTER 4: FUTURE WORK AND POTENTIAL APPLICATIONS

The central idea behind this research is that polymers that are modified through physical processes like precipitation or coalescence from their CD-ICs, with the ability to rapidly re-organize from their melts, can be used as self-nucleating agents. This study was intended to experimentally demonstrate the principle of self-nucleation in PET, using p-PET modified *via* precipitation as a self-nucleating agent in the melt-crystallization of asr-PET. Obvious extension of this work would be to conduct similar research with other polymers, since self-nucleation presents a cleaner and more "eco-friendly" way of improving properties of bulk polymer materials without using using incompatible and toxic nucleating agents, which also cause recycling difficulties. [35]

In the present study parameters like particle size of the self-nucleant (p-PET) and its uniform distribution during nucleation have not been investigated, and it would be worthwhile to see their effects on the properties of nuc-PET. Also it will be interesting to see if p-PET could be directly melt-injected and mixed into an asr-PET melt to get better mixing, and if nucleation would be improved.

PET is used in various applications, such as fibers, films, tire cords, etc. Since nuc-PET has better properties it can be potentially used as a replacement for asr-PET to make more durable products. PET is used on a large scale in packaging, specifically in bottling applications; nuc-PET not only presents a stronger more recyclable option, but also is significantly less permeable to CO_2, which is important for bottles containing carbonated

liquids. Since nuc-PET has higher stiffness and hardness than the asr-PET, it is important to consider formation and physical testing of fibers and films of nuc-PET.

Another possibility would be to make bi-component fibers and self-reinforced composites, where nuc-PET is used as reinforcement for an asr-PET matrix [44]. Such nuc-PET/asr-PET composites should have strong interfaces and physical properties superior to those of asr-PET.

REFERENCES

1. K. J. Saunders. Organic Chemistry of Polymers. *Chapman & Hall*, New York (1989)
2. D. Kint and S. Guerra, Polym Int 48: 346-352 (1999)
3. F. Awaja and D. Pavel, European Polymer Journal 41: 1453–1477 (2005)
4. P. M. Morse. Chemical Engineering News, 10: 8-14 (1997)
5. L. E. Ambroski and D. W. Flierl. Industrial & Engineering Chemistry, 45: 2290-2295 (1953)
6. Y. Kong and J. N. Hay. European Polymer Journal, 43: 1721-1727 (2003)
7. Y. Kong and J. N. Hay, Polymer, 43: 3873-3878 (2002)
8. R. Séguéla, Polymer 34: 1761-1764 (1993)
9. D. J. Sekelik, E. V. Stepanov, S. Nazarenko, D. Schiraldi, A. Hiltner and E. Baer, Journal of Polymer Science: Polymer Physics Edition, 37: 847-857 (1999)
10. S. B. Lin and J. L. Koenig, Journal of Polymer Science: Polymer Physics Edition, 20: 2277-2295 (1982)
11. J. S. Foot, I. M. Ward, Journal Of Material Science 10: 955-960 (1975)
12. J. M. Huang, P. P. Chu and F. C. Chang, Polymer, 41: 1741-1748 (2000)
13. C. J. Heffelfinger and P. G. Schmidt, Journal of Applied Polymer Science 9: 2661-2680 (1965)
14. W. H. Lee, H. Ouyang, M. C. Shih and M. H. Wu, Journal of Polymer Science: Polymer Physics Edition, 10: 133-137 (2003)
15. J. Radhakrishnan and A. Kaito, Polymer, 42: 3859-3866 (2001)
16. C. Freure, G. Chen and J. H Hortan, Surface Science, 437: 231-238 (1999)

17. H. Ouyang, W. H. Lee, S.T. Shuie and T. M. Wu, Macromolecules, 37: 7719-7723 (2004)
18. H. Ouyang, W. H. Lee and M. C. Shih, Macromolecules, 35: 8428-8432 (2002)
19. A.Villiers, Comptes Rendus de l'Acad´emie des, 112: 536-538 (1891)
20. F. Schardinger, Zeitschrift f¨ur Untersuchung der Nahrungs- und Genußmittel, 6: 865-880 (1903)
21. R. J. Freudenberg, Justus Liebigs Annalen der Chemie, 518: 102-108 (1935)
22. F.Cramer, Inclusion Compounds. Berlin: Springer-Verlag (1954)
23. J. Szejtli, Cyclodextrin Technology. Budapest: Kluwer (1988)
24. C. C. Rusa, T. Uyar, M. Rusa, M. A. Hunt, X. Wang, A. E. Tonelli, Journal of Polymer Science Part B: Polymer Physics 42: 4182–4194 (2004)
25. T. A. Bullions, M. Wei, F. E. Porbeni, M. J. Gerber, J. Peet, M. Balik, J. L. White, A. E. Tonelli, Journal of Polymer Science: Part B: Polymer Physics, 40: 992–1012 (2002)
26. T. Uyar, C. Rusa, M. Hunt, E. Aslan, J. Hacaloglu,; A. Tonelli, Polymer, 46: 4762-4775 (2005)
27. M. Wei, T. A. Bullions, C. C. Rusa, X. Wang, A. E. Tonelli, Journal of Polymer Science: Part B: Polymer Physics, 42: 386–394 (2004)
28. J. Vedula, A. E. Tonelli, Journal of Polymer Science: Part B: Polymer Physics, 45: 735–746 (2007)
29. X. L. Jiang, S. J. Luo1, K. Sun, X. D. Chen, eXPRESS Polymer Letters, 1: 245–251 (2007)
30. J. Menczel, J. Varga, Journal of Thermal Analysis, 28: 161-174 (1983)

31. H. N. Beck, H. D. Ledbetter., Journal of Applied Polymer Science, 9: 2131–2142 (1965)

32. J. P. Mercier, Polymer Engineering and Science, 30: 270–278 (1990)

33. D. Garcia, Journal of Polymer Science: Polymer Physics Edition, 22: 2063-2072 (1984)

34. A .Mohan, A. Gurarslan, X. Joyner, R. Child, A. E. Tonelli, Polymer, 52: 1055-1062 (2011).

35. L. E. Åmand and C. J. Tullin. The Theory Behind FTIR analysis, (1996)

36. J. Kenkel. Analytical Chemistry for Technicians 3rd edition (2005)

37. B. Williamson. Polymers Processed with Cyclodextrin; (2010)

38. C. Saujanya and S. Radhakrishnan, Polymer, 42: 6723-6731 (2001)

39. O. Brennan, O. D. Kennedy, T. C. Lee, S. M. Rackard, F. J. O'Brien, Journal of Biomechanics, 42: 498-503 (2009)

40. M. H. Litt; P. J. Koch; A. V. Tobolsky, Journal of Macromolecular Science, Part B, 1: 587 – 594 (1967)

41. J. E. Mark. Polymer Data Handbook, p-558 (1999)

42. B.D.Blake, G.J.Leggett; Polymer 43: 319-327 (2002)

43. A. Gurarslan, A. E. Tonelli, Macromolecules, 44: 3856–3861 (2011)